

Water Oxidation by an Electropolymerized Catalyst on Derivatized Mesoporous Metal Oxide Electrodes

Dennis L. Ashford,[†] Alexander M. Lapides,[†] Aaron K. Vannucci, Kenneth Hanson, Daniel A. Torelli, Daniel P. Harrison, Joseph L. Templet,* Thomas J. Meyer*

Department of Chemistry, University of North Carolina at Chapel Hill, CB 3290, Chapel Hill, North Carolina 27599, United States

Contents

1. Experimental Section.....	Page S3
2. Figure S1. Crystal structure of Ru-NCC₃²⁺	Page S5
3. Figure S2. <i>PolyRuOH₂²⁺</i> surface coverage on <i>p</i> FTO and <i>p</i> FTO- RuPdvb²⁺	Page S6
4. Figure S3. <i>i_{peak}</i> for <i>polyRu^{III/II}OH₂</i> couple versus scan rate	Page S6
5. Figure S4. <i>E_{1/2}</i> versus pH of <i>p</i> FTO- RuPdvb²⁺-polyRuOH²⁺	Page S7
6. Figure S5. UV/Visible spectrum of RuOH₂²⁺ in H ₂ O.....	Page S7
7. Figure S6. UV/Visible spectra of <i>n</i> TiO ₂ following electropolymerization of RuOH₂²⁺	Page S8
8. Figure S7. UV/Visible spectra of <i>n</i> TiO ₂ - RuPdvb²⁺ before and after electropolymerization of RuOH₂²⁺	Page S9
9. Figure S8. Cross-sectional SEM images of <i>n</i> TiO ₂ - RuPdvb²⁺ following 60, 120, and 450 reductive cycles of RuOH₂²⁺	Page S9
10. Figure S9. EDS spectra of <i>n</i> TiO ₂ - RuPdvb²⁺-polyRuOH₂²⁺ following 450 reductive cycles.....	Page S10
11. Figure S10. Changes in the UV/Visible spectrum of <i>n</i> TiO ₂ - RuP and <i>n</i> TiO ₂ - RuPdvb²⁺-polyRuOH₂²⁺ under 455 nm irradiation.....	Page S10
12. Figure S11. Changes in the UV/Visible spectrum of <i>n</i> TiO ₂ - RuP and <i>n</i> TiO ₂ - RuPdvb²⁺-polyRuOH₂²⁺ under 455 nm irradiation.....	Page S11
13. Figure S12. Spectroelectrochemistry of <i>n</i> ITO- RuPdvb²⁺-polyRuOH₂²⁺	Page S12
14. Figure S13. CVs of <i>n</i> ITO- <i>polyRuOH₂²⁺</i> and <i>n</i> ITO- RuPdvb²⁺-polyRuOH₂²⁺	Page S13
15. Figure S14. Plots of <i>i_c/i_p</i> versus 1/ <i>v</i> for <i>n</i> ITO- <i>polyRuOH₂²⁺</i> , <i>n</i> ITO- RuPdvb²⁺-polyRuOH₂²⁺ , and <i>n</i> ITO- <i>polyRuOH₂²⁺</i> and <i>n</i> ITO- RuPOH₂²⁺	Page S14
16. Figure S15. Plots of <i>i_c/i_p</i> versus 1/ <i>v</i> for <i>p</i> FTO- <i>polyRuOH₂²⁺</i> , and <i>p</i> FTO- RuPdvb²⁺-polyRuOH₂²⁺	Page S15

17. Figure S16. Gas chromatographs of headspace following controlled potential electrolysis...Page S15
18. Figure S17. CVs of *n*ITO-**RuPdvb**²⁺-*polyRuOH*₂²⁺ before and after 2 hr electrolysis.....Page S16
19. Figure S18. CVs of *n*ITO-**RuPdvb**²⁺-*polyRuOH*₂²⁺ before and after 14 hr electrolysis..... Page S16
20. Structural information for single crystal analysis of **Ru-NCCH**₃²⁺Page S17

Experimental

Sample Preparation.

Materials. $[\text{Ru}(\eta^6\text{-benzene})(\text{Cl})_2]_2$,¹ 2,6-bis(1-methyl-1H-benzo[d]imidazol-2-yl)pyridine,² and 5,5'-divinyl-2,2'-bipyridine³ were synthesized as previously reported. Distilled water was further purified by using a Milli-Q Ultrapure water purification system. All other reagents were ACS grade and used without further purification. Fluoride-doped tin oxide (FTO)-coated glass (Hartford Glass; sheet resistance $15 \Omega \text{ cm}^{-2}$) was cut into $10 \text{ mm} \times 40 \text{ mm}$ strips and used as the substrate for TiO_2 nanoparticle films. Microwave reactions were carried out using a CEM MARS microwave reactor. A CEM HP-500 Plus Teflon-coated microwave vessel (100 mL) was used at a power setting of 400 W. The vessel was rotated and stirred throughout the microwave procedure. The pressure of the reaction vessel was monitored throughout the reaction, and never exceeded 300 PSI.

Metal Oxide Films. $n\text{TiO}_2$ films, typically $4 - 7 \mu\text{m}$ thick ($\sim 20 \text{ nm}$ particle diameter), with a coating area of roughly $10 \text{ mm} \times 15 \text{ mm}$, were synthesized according to a literature procedure.⁴

Electrochemical and Photophysical Measurements.

Absorption spectra were obtained by placing the dry derivatized films perpendicular to the detection beam path of the spectrophotometer. The expression, $\Gamma = A(\lambda)/\varepsilon(\lambda)/1000$, was used to calculate surface coverages.⁵ Molar extinction coefficients (ε) in H_2O were used; $A(\lambda)$ was the absorbance at the MLCT λ_{\max} . All measurements were carried out of films loaded from methanol solutions of $150 \mu\text{M}$ in ruthenium complex, which gave complete surface coverage ($\Gamma = 8 \times 10^{-8} \text{ mol cm}^{-2}$).

Electrochemical measurements were conducted on a CH Instruments 660D potentiostat with a Pt-mesh or Pt-wire counter electrode, and a Ag/AgNO_3 (0.01 M AgNO_3 /0.1 M tetra-n-butylammonium hexafluorophosphate (TBAPF₆) in CH_3CN ; -0.09 V vs. $\text{Fc}^{+/\text{0}}$)⁶ or Ag/AgCl (3 M NaCl; 0.197 V vs. NHE) reference electrode. $E_{1/2}$ values were obtained from the peak currents in square wave voltammograms or from averaging cathodic and anodic potentials at peak current values ($E_{p,c}$ and $E_{p,a}$) in cyclic voltammograms. Reductive electropolymerization was carried out in anhydrous propylene carbonate (dried over MgSO_4) with 0.1 M tetrabutylammonium hexafluorophosphate (TBAPF₆) as the supporting electrolyte under an atmosphere of argon. Solutions were degassed with argon for at least 5 minutes prior to reductive electrochemical cycling.

Surface coverages on planar FTO electrodes were calculated using Eq. S1 where Q is the integrated current under the $\text{Ru}^{\text{III}/\text{II}}\text{-OH}_2$ redox couple of polyRuOH_2^{2+} , F is Faraday's constant (96,485 C), n is the number of electrons transferred ($n = 1$), and A is the area of the electrode ($\sim 1 \text{ cm}^2$).

$$\Gamma = Q/nFA \quad (\text{Eq. S1})$$

Catalytic rate constants for the water oxidation, k_{obs} , were calculated using Eq. S2 where i_{cat} is the catalytic current taken at 1.7 V (vs NHE), i_{peak} is the current taken for the $\text{Ru}^{\text{III}}\text{-OH}/\text{Ru}^{\text{II}}\text{-OH}_2$ redox couple, n_{cat} is the number of electrons involved in the catalytic step (4 for water oxidation), R is the ideal gas constant, T is the temperature, n_p is the number of electrons involved in the $\text{Ru}^{\text{III}}\text{-OH}/\text{Ru}^{\text{II}}\text{-OH}_2$ redox couple (1 in this case), F is Faraday's constant, and v is the scan rate.

$$\frac{i_{\text{cat}}}{i_{\text{peak}}} = \left(\frac{4RTn_{\text{cat}}}{n_p^2 F} \right) k_{\text{obs}} \left(\frac{1}{v} \right) \quad (\text{Eq. S2})$$

Scanning electron microscopy (SEM) and energy dispersive X-ray spectroscopy (EDS) results were obtained on a FEI Helios 600 Nanolab Dual Beam System equipped with an Oxford instruments, INCA PentaFET-x3 detector. A cross section was taken of $n\text{TiO}_2\text{-RuPdvB}^{2+}$ that had been reductively cycled 60, 120, and 300 times in presence of RuOH_2^{2+} . Surface images were taken at 5 kV with a 86 pA beam current. Three EDS spectra were obtained at the $\text{TiO}_2/\text{solution}$ interface (top), in the bulk of TiO_2 nanoparticles (middle), and at the nano- TiO_2/FTO interface (bottom) of the cross section.

Photostability measurements were performed by a previously reported procedure.⁸ The light from a Royal Blue (455 nm, FWHM $\sim 30 \text{ nm}$, 475 mW/cm²) Mounted High Power LED (Thorlabs, Inc., M455L2) powered by a T-Cube LED Driver (Thorlabs, Inc., LEDD1B) was focused to a 2.5 mm diameter spot size by a focusing beam probe (Newport Corp. 77646) outfitted with a second lens (Newport, Corp 41230). The light output was directed onto the derivatized thin film placed at 45° in a standard 10 mm path length cuvette containing 3 mL of the solution. The illumination spot was adjusted to coincide both with the thin film and the perpendicular beam path of a Varian Cary 50 UV/Vis spectrophotometer. The absorption spectrum (360 – 800 nm) of the film was taken every 15 minutes over 16 hours of illumination. The incident light intensity was measured with a thermopile detector (Newport Corp 1918-C meter and 818P-020-12 detector). The solution temperature, $22 \pm 2^\circ\text{C}$, was consistent throughout the duration of the experiment.

The absorption-time traces at 400 nm, 450 nm, and 500 nm for the pH 4.6 (0.1 M HOAc/OAc, 0.5 M NaClO₄) could be satisfactorily fit with the biexponential function (Eq. S3). For comparison purposes, the results of the multi-exponential analysis were represented by a single rate constant by first calculating the weighted average lifetime ($\langle\tau\rangle$) using Eq. S4. The three weighted average lifetimes ($\langle\tau\rangle_{400\text{nm}}, \langle\tau\rangle_{450\text{nm}}, \langle\tau\rangle_{500\text{nm}}$) were then averaged (Eq. S5) to give a desorption rate constant k_{des} .

$$y = A_1 e^{-(1/1)x} + A_2 e^{-(1/2)x} + y_0 \quad (\text{eq S3})$$

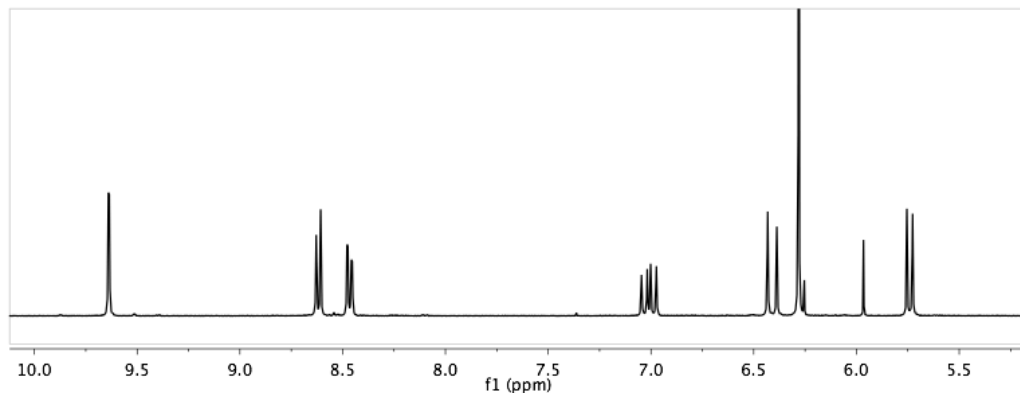
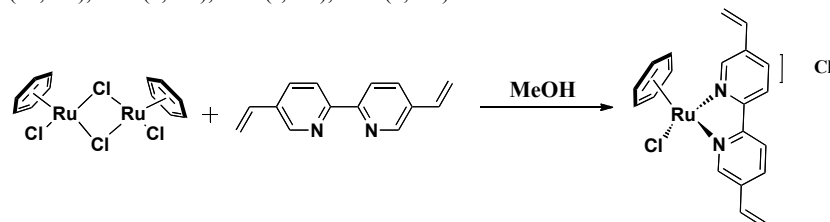
$$\langle \tau \rangle = \sum A_i \tau_i^2 / \sum A_i \quad (\text{eq S4})$$

$$1/k_{\text{des}} = (\langle \tau \rangle_{400\text{nm}} + \langle \tau \rangle_{450\text{nm}} + \langle \tau \rangle_{500\text{nm}}) / 3 \quad (\text{Eq. S5})$$

Synthesis.

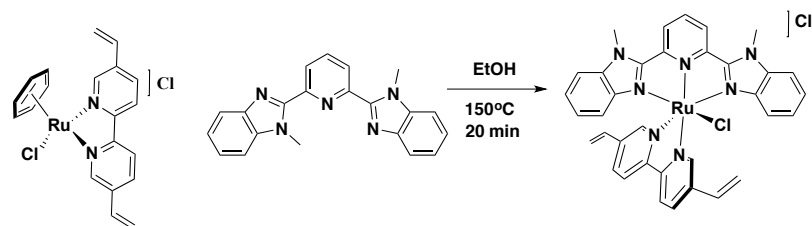
[Ru(5,5'-dvb)(η⁶-benzene)(Cl)](Cl)

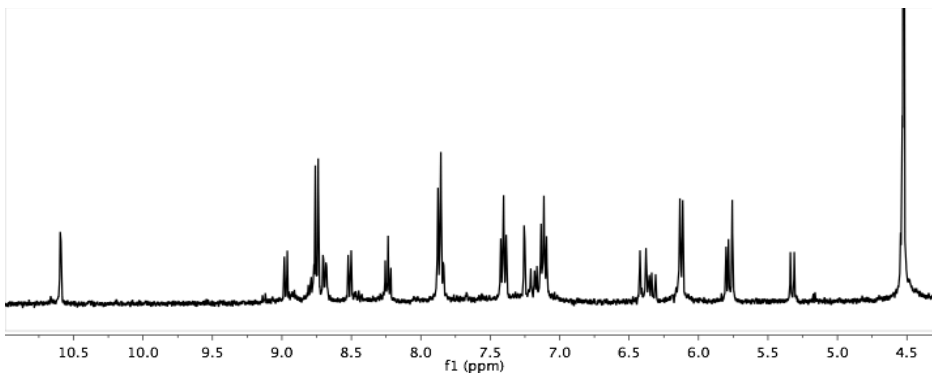
This complex was synthesized according a modified literature procedure.⁹ [Ru(η⁶-benzene)(Cl)₂]₂ (0.24 g, 0.48 mmol) and 5,5'-divinyl-2,2'-bipyridine (0.2 g, 0.96 mmol) were dissolved in MeOH (~40 mL). The solution was refluxed overnight under an atmosphere of argon. The reaction was cooled, filtered, and the filtrate was taken to dryness by a rotary evaporator. The solid was triturated with ether, collected, and air-dried. This complex was used without further purification (0.42 g, 95%). ¹H NMR (400 MHz, DMSO) δ (ppm) 9.64 (s, 2H), 8.63 (d, 2H), 8.48 (d, 2H), 7.05 (dd, 2H), 6.43 (d, 2H), 6.28 (s, 6H), 5.73 (d, 2H).



[Ru(Mebimpy)(5,5'-dvb)(Cl)](Cl)

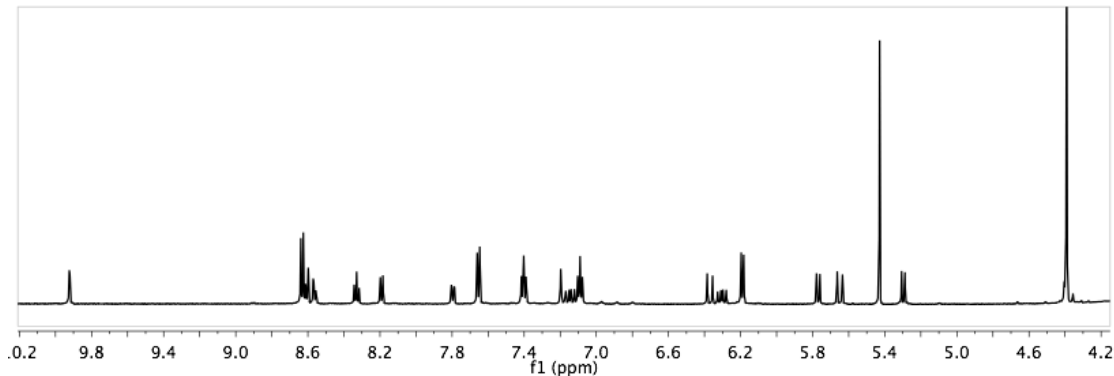
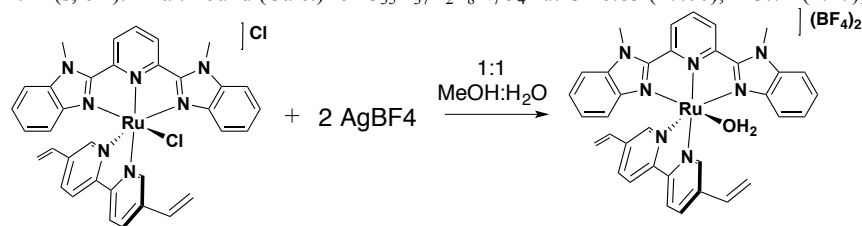
This complex was synthesized according a modified literature procedure.¹⁰ [Ru(5,5'-dvb)(η⁶-benzene)(Cl)]Cl (0.122 g, 0.27 mmol) and 2,6-bis(1-methyl-1H-benzo[d]imidazol-2-yl)pyridine (0.09 g, 0.27 mmol) were heated at reflux for 20 minutes at 150 °C in 40 mL EtOH in a microwave reactor. The solution was cooled, then filtered. A saturated solution of LiCl (~15 mL) was added along with additional H₂O (15 mL), and the EtOH was removed by rotary evaporation. The dark purple precipitate was filtered, washed with water and ether, air dried and collected. This complex was used without further purification (0.169 g, 87%). ¹H NMR (600 MHz, d₆-DMSO) δ (ppm) 10.6 (s, 1H), 8.98 (d, 1H), 8.76 (m, 2H), 8.70 (d, 1H), 8.50 (d, 1H), 8.24 (t, 1H), 7.87 (m, 3H), 7.40 (t, 2H), 7.26 (s, 1H), 7.11 (m, 3H), 6.42 (d, 1H), 6.32 (d, 1H), 6.11 (d, 2H), 5.79 (m, 2H), 5.32 (d, 1H), 4.53 (s, 6H).





[Ru(Mebimpy)(5,5'-dvb)(OH₂)](BF₄)₂ (**RuOH₂²⁺**)

[Ru(Mebimpy)(5,5'-dvb)(Cl)](Cl) (0.344 g, 0.48 mmol) was dissolved in 1:1 MeOH:H₂O (~ 30 mL) under an atmosphere of argon. A solution of AgBF₄ (0.189 g, 0.97 mmol) in H₂O (~10 mL) was added. The solution was refluxed in the dark overnight under an atmosphere of argon. The solution was cooled, filtered through Celite, and the filtrate was taken to dryness using a rotary evaporator. The crude product was then purified by size-exclusion chromatography (Sephadex LH-20) with 1:1 MeOH:H₂O as eluent. Similar fractions (based of UV-Vis spectra) were combined, and the solvent was removed by rotary evaporation. The dark red solid was triturated with ether and collected (0.29 g, 73%). ¹H NMR (600 MHz, CD₃CN) δ (ppm) 9.97 (s, 1H), 8.60 (m, 4H), 8.34 (t, 1H), 8.19 (d, 1H), 7.82 (dd, 1H), 7.67 (d, 2H), 7.44 (t, 2H), 7.22 (d, 1H), 7.18 (dd, 1H), 7.12 (t, 2H), 6.42 (d, 1H), 6.36 (dd, 1H), 6.23 (d, 2H), 5.80 (d, 1H), 5.69 (d, 1H), 5.33 (d, 1H), 4.41 (s, 6H). Anal. Found (Calc.) for C₃₅H₃₇B₂F₈N₇O₄Ru: C 46.83 (47.00), H 3.72 (4.17), N 10.96 (10.96).



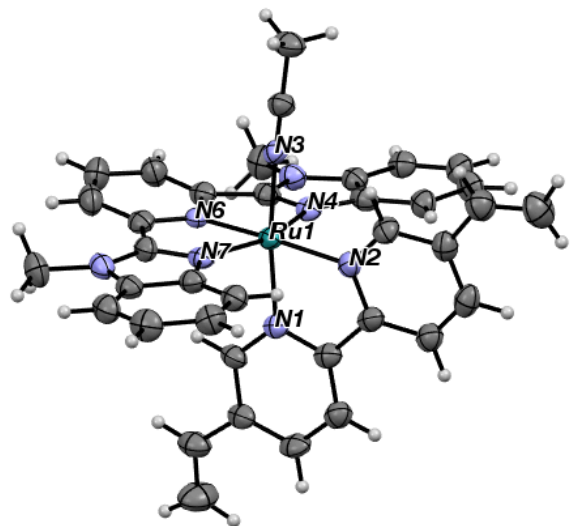


Figure S1. Crystal structure of **Ru-NCCCH₃²⁺** grown by slow diffusion of diethyl ether into a solution of **RuOH₂²⁺** in CH₃CN. Structural details are listed at the end of Supporting Information.

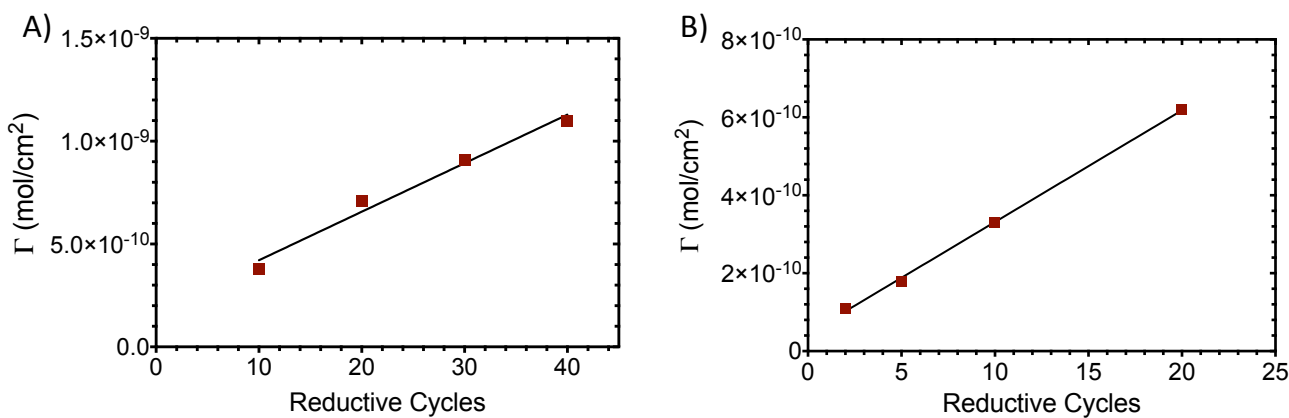


Figure S2. PolyRuOH₂²⁺ surface coverage on (A) bare pFTO and (B) pFTO-RuPdvb²⁺ versus the number of reductive cycles in dry PC solution of RuOH₂²⁺ (0.5 mM, 0.1 M TBAPF₆), cycling form 0 to -1.8 V (vs. Ag/AgNO₃), Pt counter, and Ag/AgNO₃ reference electrode.

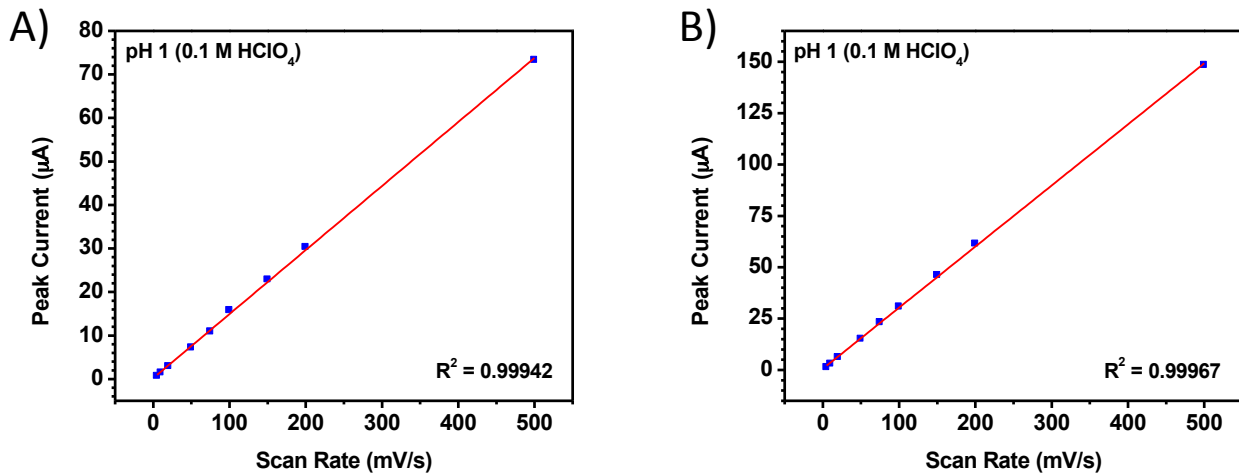


Figure S3. Peak current for the $\text{polyRu}^{\text{III}/\text{II}}\text{OH}_2$ redox couple versus the scan rate for $p\text{FTO-RuPdvb}^{2+}$ - polyRuOH_2^{2+} with 5 (A) and 20 (B) monolayers of polyRuOH_2^{2+} in aqueous 0.1 M HClO_4 , Pt-wire counter electrode, and Ag/AgCl reference electrode.

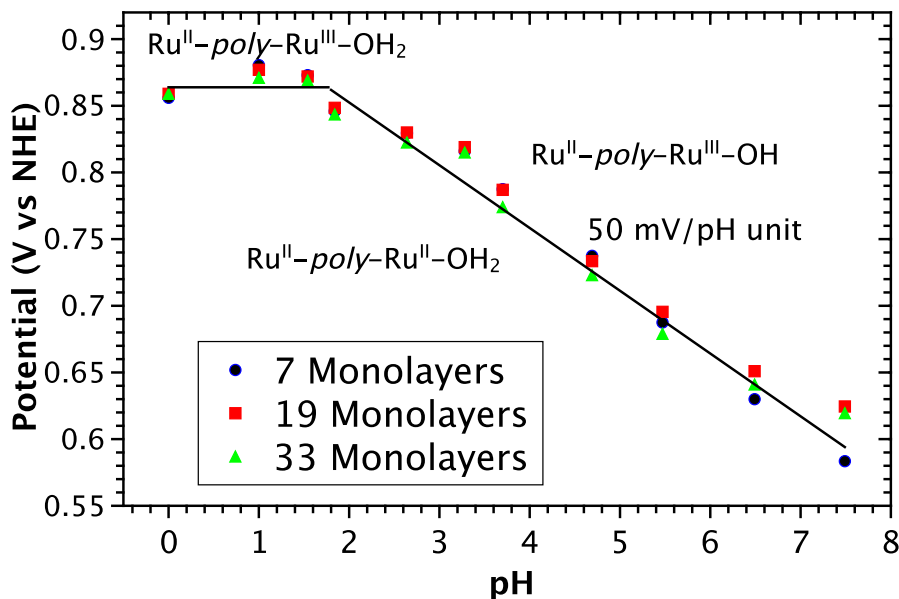


Figure S4. $E_{1/2}$ versus pH diagram of $p\text{FTO-RuPdvb}^{2+}$ - polyRuOH_2^{2+} with 7 (blue circles), 19 (red squares) and 33 (green triangles) monolayer equivalents of RuOH_2^{2+} deposited onto $p\text{FTO-RuPdvb}^{2+}$. $E_{1/2}$ values were obtained at peak current maxima in square wave voltammograms. The solid lines are best fits of the variation in $E_{1/2}$ values with pH for the $\text{Ru}^{\text{III}}\text{-OH}_2/\text{Ru}^{\text{II}}\text{-OH}_2$ and $\text{Ru}^{\text{III}}\text{-OH}/\text{Ru}^{\text{II}}\text{-OH}_2$ redox couples at 23 °C in aqueous 0.5 M NaClO_4 and 0.1 M buffer.

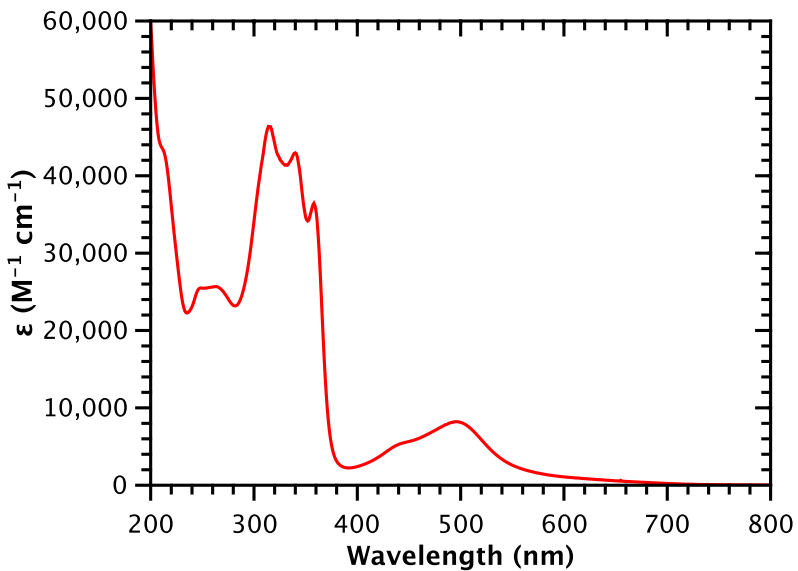


Figure S5. Absorption spectrum of RuOH_2^{2+} at room temperature in H_2O .

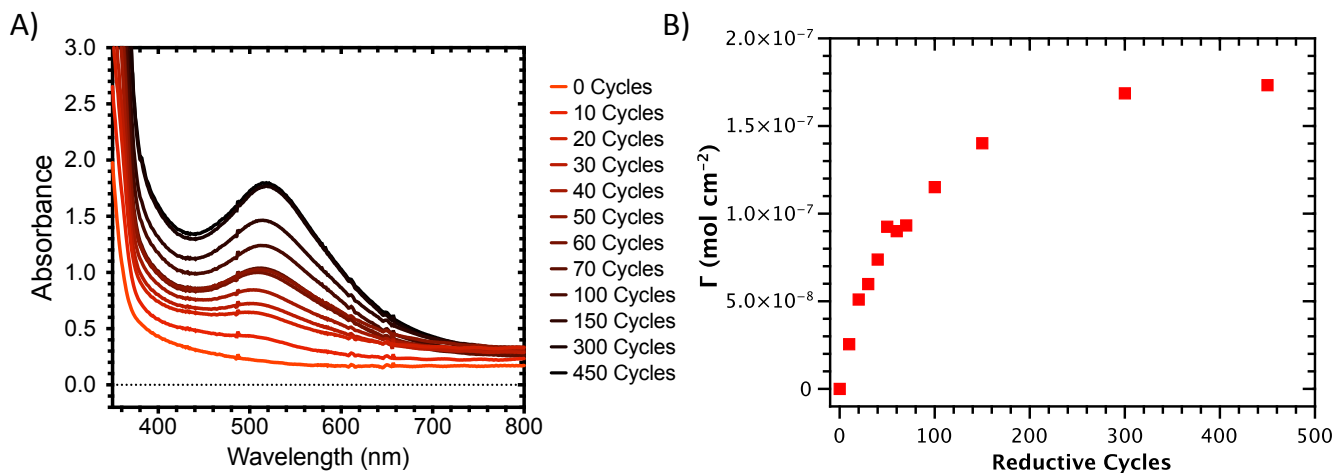


Figure S6. (A) Changes in UV/visible absorption spectra for $n\text{TiO}_2$ with increasing number of reductive cycles from 0 to -1.8 V (vs Ag/AgNO_3) in PC solution (0.1 M TBAPF₆) of RuOH_2^{2+} (0.5 mM), Pt counter, and Ag/AgNO_3 reference. (B) Surface coverage of polyRuOH_2^{2+} versus the number of reductive cycles.

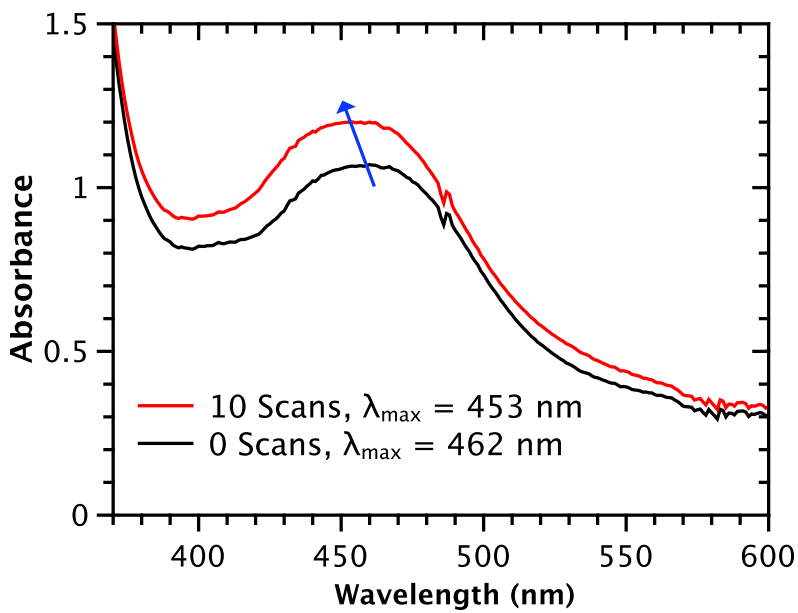


Figure S7. UV-visible absorption spectra of $n\text{TiO}_2\text{-RuPdvb}^{2+}$ before (black) and after (red) 10 reductive cycles from 0 to -1.8 V (vs Ag/AgNO₃) in a PC solution of 0.5 mM RuOH₂²⁺, Pt counter, and Ag/AgNO₃ reference electrode.

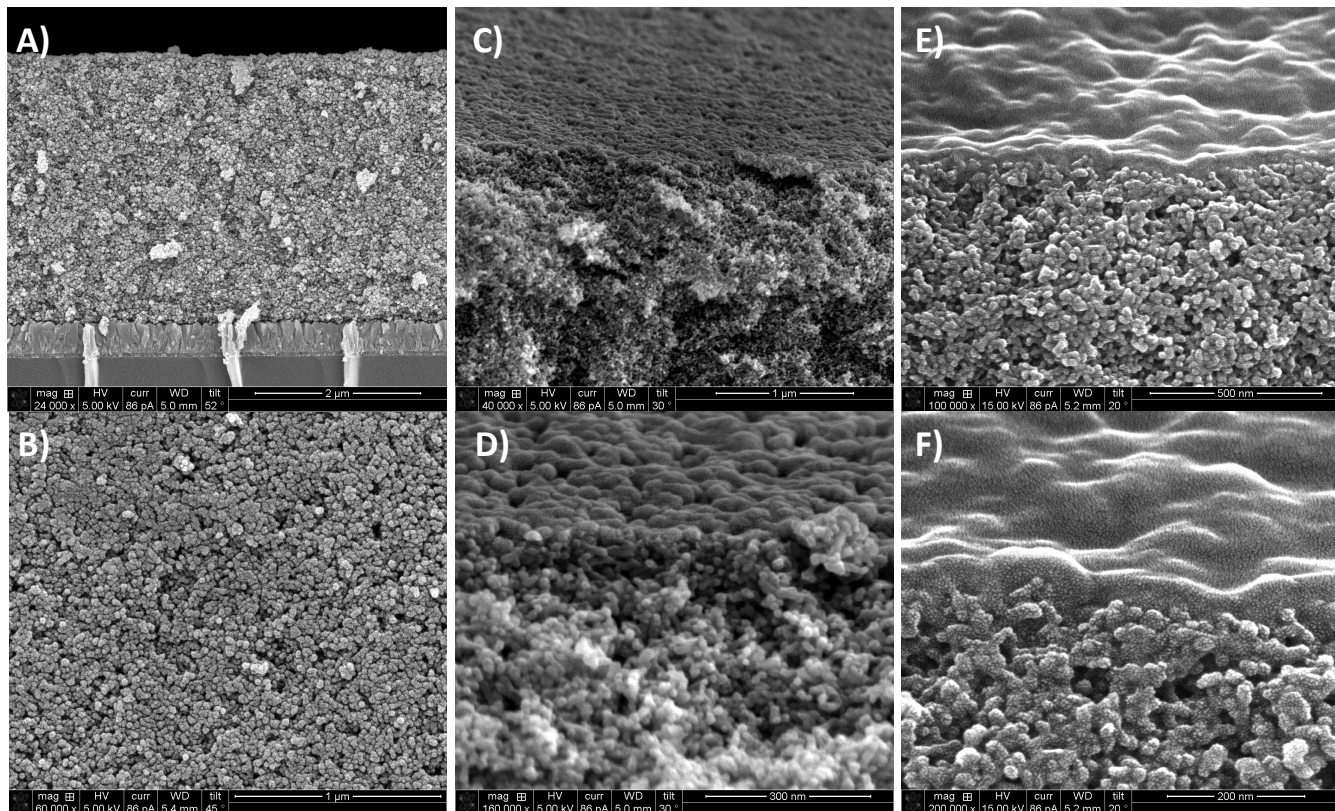
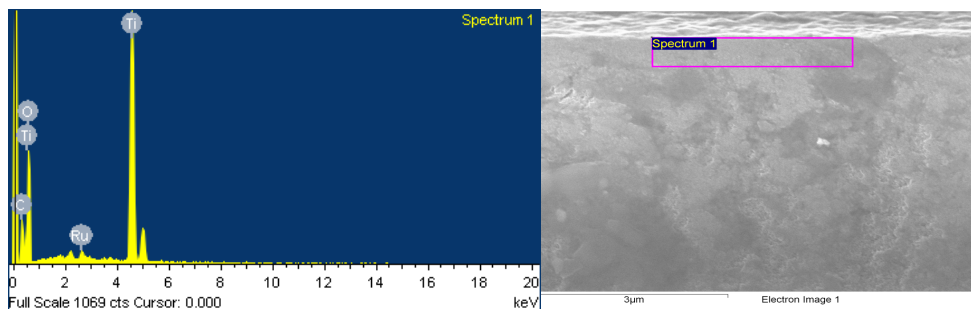
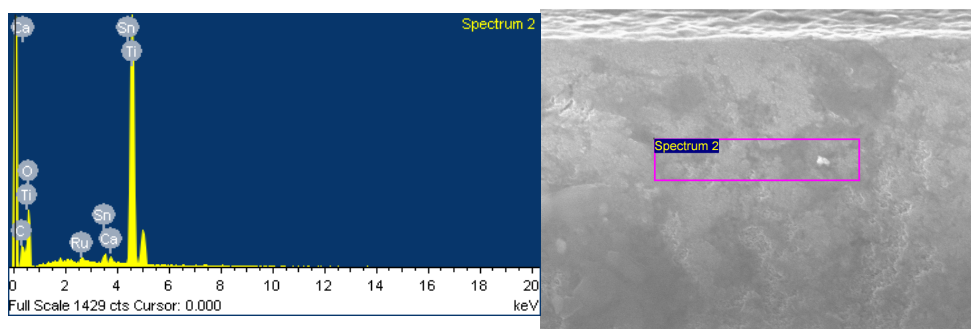


Figure S8. Cross-sectional SEM images of the $n\text{TiO}_2\text{-RuPdvb}^{2+}$ films following 60 (A and B), 120 (C and D), and 450 (E and F) reductive cycles in a PC solution containing 0.5 mM RuOH₂²⁺.

Element	Weight%	Atomic%
C K	12.07	19.68
O K	54.70	66.98
Ti K	32.03	13.10
Ru L	1.19	0.23
Totals	100.00	



Element	Weight%	Atomic%
C K	7.64	14.27
O K	46.42	65.14
Ca K	0.42	0.23
Ti K	41.90	19.64
Ru L	1.06	0.24
Sn L	2.56	0.48
Totals	100.00	



Element	Weight%	Atomic%
C K	5.44	11.44
O K	40.44	63.91
Si K	1.81	1.63
Ti K	37.62	19.85
Ru L	0.91	0.23
Sn L	13.78	2.93
Totals	100.00	

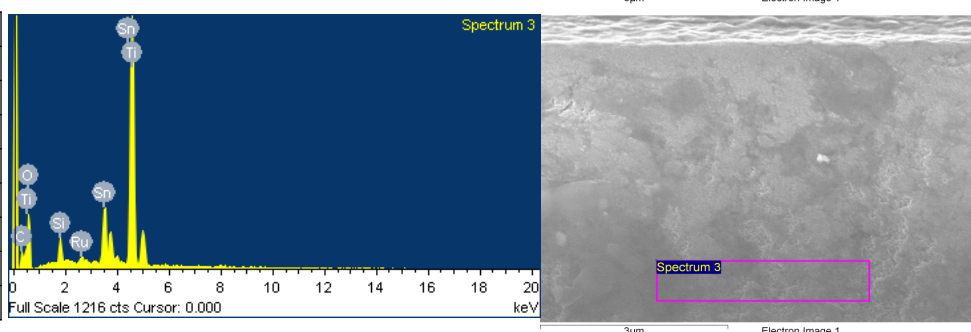


Figure S9. EDS spectra (middle) and the tabulated results (left) obtained for $n\text{TiO}_2\text{-RuPdvb}^{2+}$ - polyRuOH_2^{2+} following 450 reductive cycles at various depths that are indicated by the pink rectangle (right).

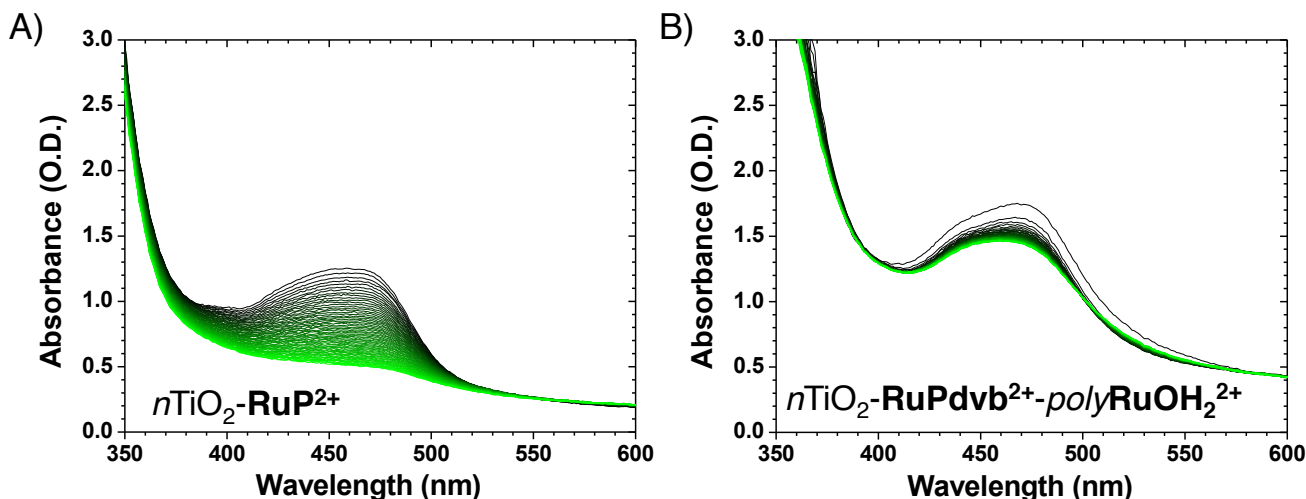


Figure S10. Changes in the absorption spectrum of $n\text{TiO}_2\text{-RuP}$ (A) and $n\text{TiO}_2\text{-RuPdvb}^{2+}$ - polyRuOH_2^{2+} following 70 reductive cycles (B, 1:1 chromophore:catalyst) in aqueous 0.1 M HClO₄ under constant 455 nm irradiation (475 mW/cm²) from 0 h (green) to 16 h (black) recorded every 15 min.

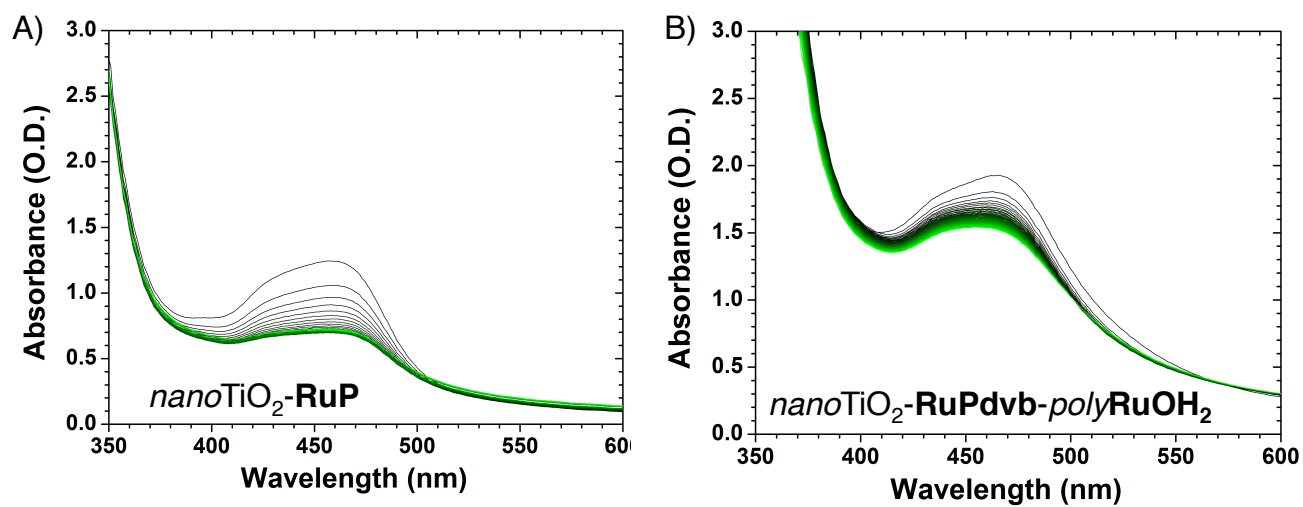


Figure S11. Changes in the absorption spectrum of *nTiO₂-RuP* (A) and *nTiO₂-RuPdvb²⁺-polyRuOH₂* (B, 1:1 chromophore:catalyst) in pH 4.7 aqueous solution (0.1 M HOAc/OAc, 0.5 M NaClO₄) under constant 455 nm irradiation (475 mW/cm²) from 0 h (green) to 16 h (black) recorded every 15 min.

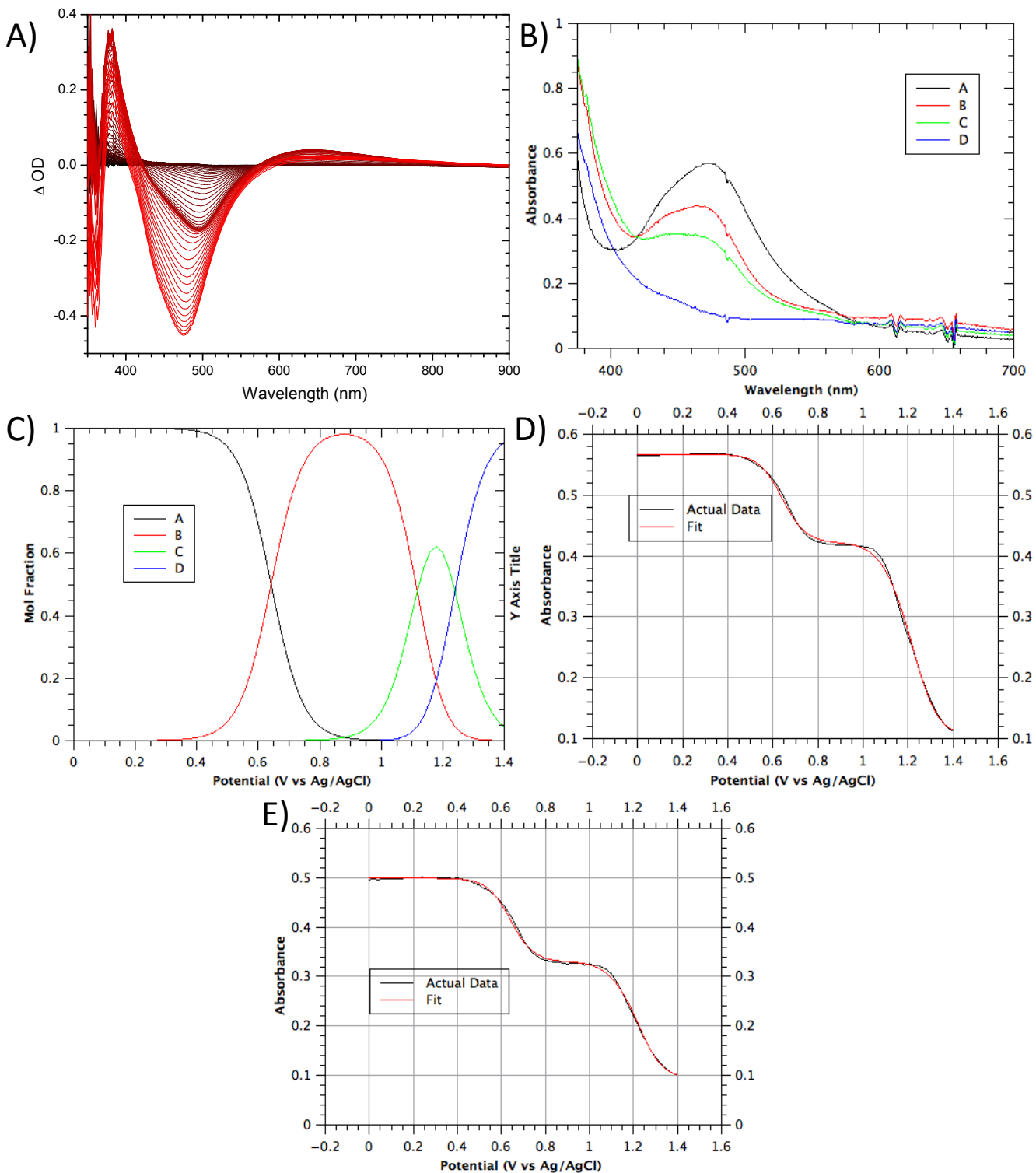


Figure S12. (A) Spectroelectrochemistry of **nITO-RuPdvb²⁺-polyRuOH₂²⁺** in 0.1 M HClO₄ with a Pt-mesh counter electrode and Ag/AgCl reference electrode. The **nITO-RuPdvb²⁺-polyRuOH₂²⁺** slide was stepped 0.02 V and held there for 300 s. Following each potential step, a UV/Visible spectrum of the slide was obtained. (B) Calculated spectra for the multiwavelength fit to the kinetic model $A \rightleftharpoons B \rightleftharpoons C \rightleftharpoons D$ with $A = [\text{Ru}^{\text{II}}\text{-Ru}^{\text{II}}\text{-OH}_2]^{4+}$, $B = [\text{Ru}^{\text{II}}\text{-Ru}^{\text{III}}\text{-OH}_2]^{5+}$, $C = [\text{Ru}^{\text{II}}\text{-Ru}^{\text{IV}}=\text{O}]^{5+}$, and $D = [\text{Ru}^{\text{III}}\text{-Ru}^{\text{IV}}=\text{O}]^{6+}$. (C) Calculated concentration profiles versus the applied potential (V vs Ag/AgCl) for the model $A \rightleftharpoons B \rightleftharpoons C \rightleftharpoons D$. (D) Changes in absorption versus potential at 476 nm ($\lambda_{\max, \text{MLCT}}$ for **RuPdvb²⁺**) in black and calculated fit (red) using the model $A \rightleftharpoons B \rightleftharpoons C \rightleftharpoons D$. (E) Changes in absorption versus potential at 491

nm ($\lambda_{\max, \text{MLCT}}$ for RuOH_2^{2+}) in black and calculated fit (red) using the model $A \rightleftharpoons B \rightleftharpoons C \rightleftharpoons D$. The data was fit using SPECFIT/32 by a series of three sequential Nernstian steps ($A \rightleftharpoons B \rightleftharpoons C \rightleftharpoons D$).

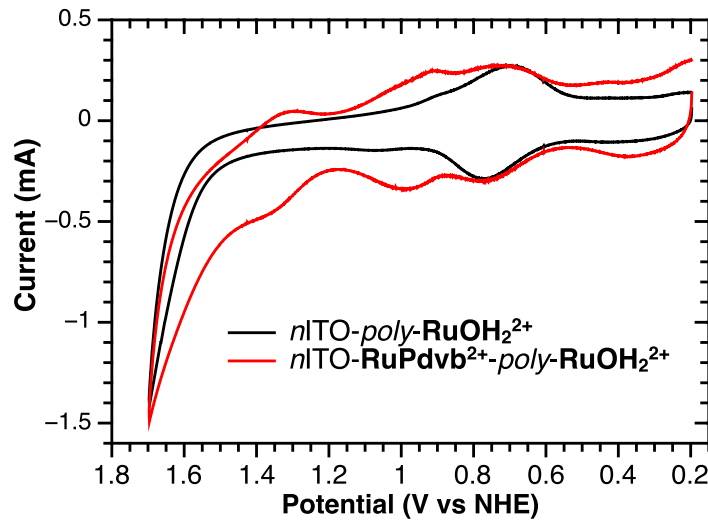


Figure S13. Cyclic voltammograms at 10 mV/s of *nITO-RuPdvb²⁺-polyRuOH₂²⁺* (red) and *nITO-polyRuOH₂²⁺* (black) in pH 4.7 aqueous solution (0.1 M HOAc/OAc, 0.5 M NaClO₄); Pt-mesh counter electrode and Ag/AgCl reference electrode. The voltammograms are normalized to the Ru^{III}-OH/Ru^{II}-OH redox couple for comparison purposes.

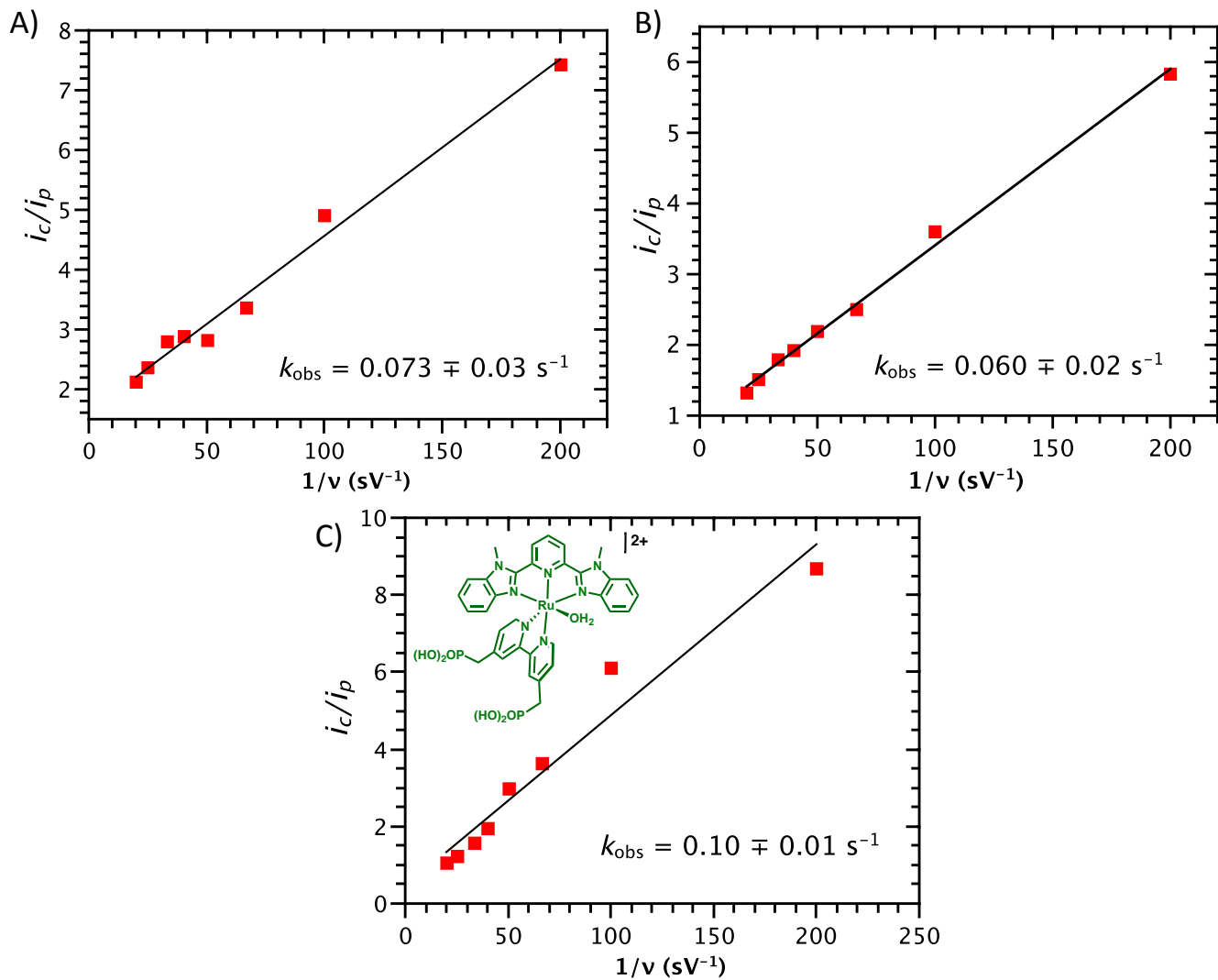


Figure S14. Plots of i_c/i_p (i_c is the current at 1.7 V vs NHE, i_p is the peak current for the $\text{Ru}^{\text{III}}\text{-OH}_2/\text{Ru}^{\text{II}}\text{-OH}_2$ redox couple) versus $1/v$ for (A) $n\text{ITO}\text{-RuPdVb}^{2+}\text{-polyRuOH}_2^{2+}$, (B) $n\text{ITO}\text{-polyRuOH}_2^{2+}$ and (C) $n\text{ITO}\text{-[Ru(Mebimpy)(4,4'-(PO}_3\text{H}_2\text{-CH}_2)_2\text{-bpy})(OH}_2\text{)]}^{2+}$ (RuPOH_2^{2+}) in pH 4.7 aqueous solution (0.1 M HOAc/OAc, 0.5 M NaClO₄); Pt-mesh counter electrode and Ag/AgCl reference electrode. Surface coverages for each complex were $\sim 1.1 \times 10^{-8} \text{ mol cm}^{-2}$ at 23 °C. The catalytic rate constant, k_{obs} , for water oxidation was evaluated from the slope of the each plot.

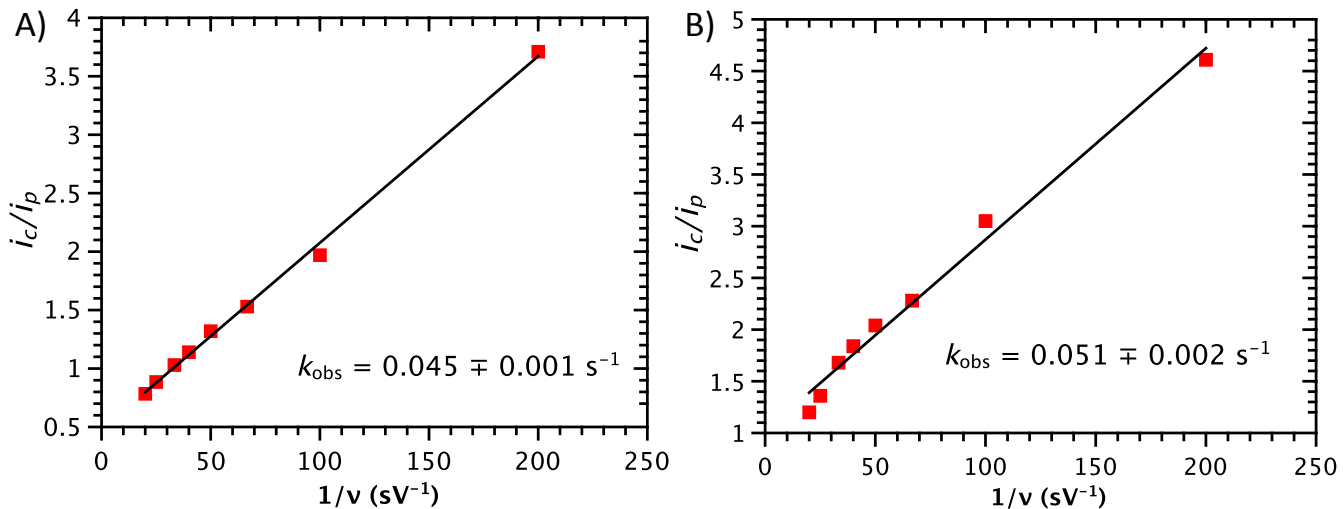


Figure S15. Plots of i_c/i_p (i_c is the current at 1.7 V vs NHE, i_p is the peak current for the Ru^{III}-OH₂/Ru^{II}-OH₂ redox couple) versus $1/v$ for (A) *p*FTO-***polyRuOH*₂₊**, and (B) *p*FTO-**RuPdvb²⁺-polyRuOH₂₊** in pH 4.7 aqueous solution (0.1 M HOAc/OAc, 0.5 M NaClO₄); Pt-mesh counter electrode and Ag/AgCl reference electrode. Surface coverages for each complex were $\sim 1 \times 10^{-10}$ mol cm⁻² at 23 °C. The catalytic rate constant, k_{obs} , for water oxidation was evaluated from the slope of the each plot.

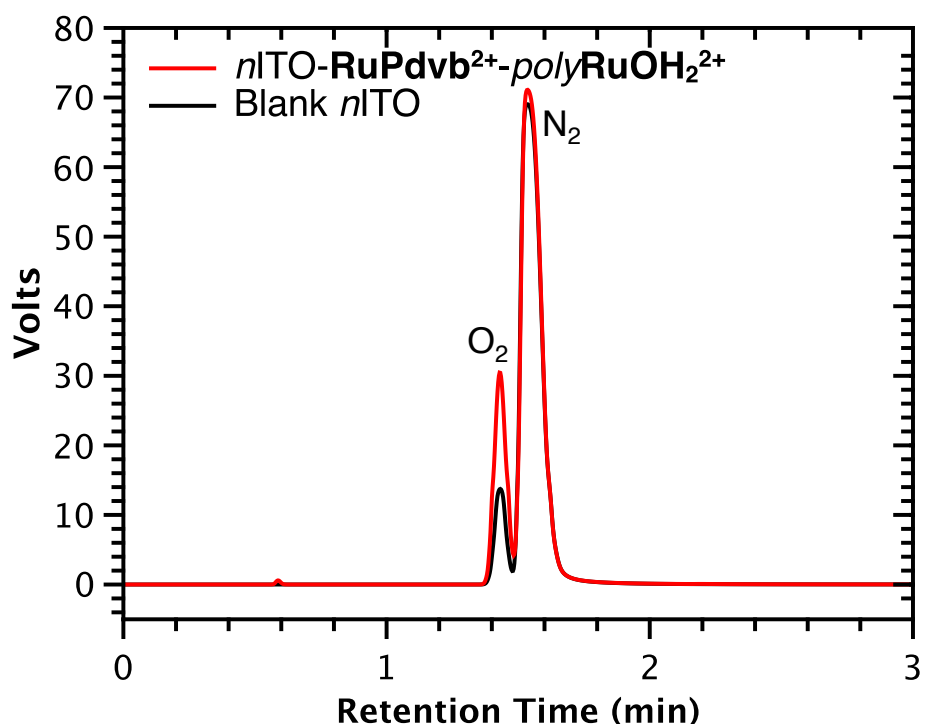


Figure S16. Gas chromatographs of headspace following electrolysis of blank *n*ITO (black) and *n*ITO-**RuPdvb²⁺-polyRuOH₂₊** (red) at 1.7 V (vs NHE) in pH 4.7 ((0.1 M HOAc/OAc, 0.5 M NaClO₄); Pt-mesh counter electrode and Ag/AgCl reference electrode. Surface coverages for both **RuPdvb²⁺** and ***polyRuOH₂₊*** were $\sim 1.1 \times 10^{-8}$ mol cm⁻².

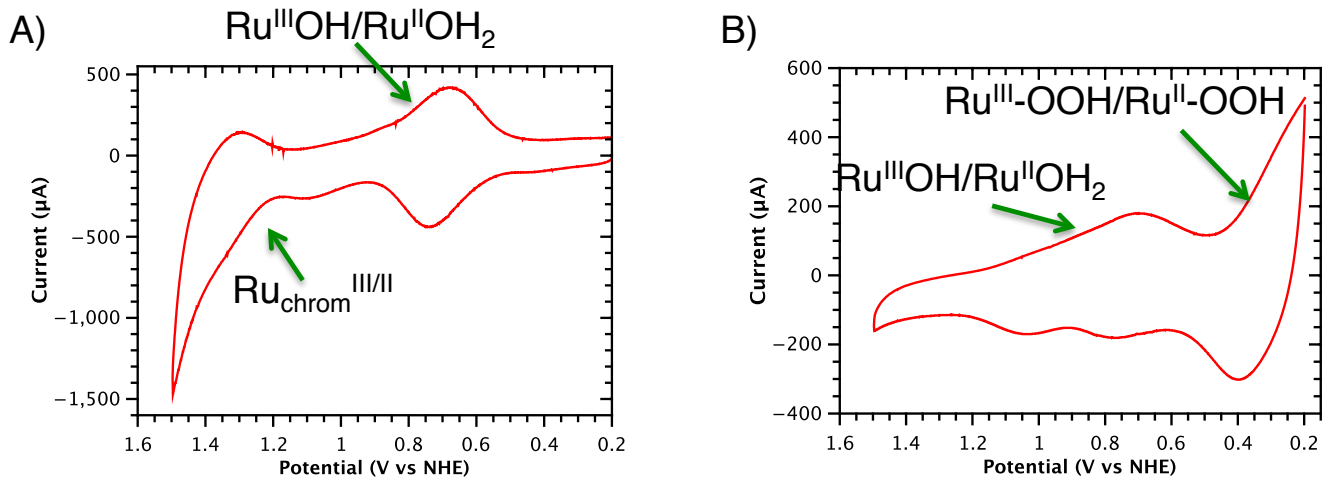


Figure S17. Cyclic voltammograms of **nITO-RuPdvb²⁺-polyRuOH₂²⁺** pre (A) and post 2 hr (B) electrolysis at 1.7 V (vs NHE) in pH 4.7 ((0.1 M HOAc/OAc, 0.5 M NaClO₄); Pt-mesh counter electrode and Ag/AgCl reference electrode. Surface coverages for both **RuPdvb²⁺** and **polyRuOH₂²⁺** were $\sim 1.1 \times 10^{-8}$ mol cm⁻² pre electrolysis. As noted in the figure, the new waves below 0.4 V are due to a peroxide intermediate in the overall water oxidation cycle. The surface coverage post electrolysis (Figure S17(B)) for **polyRuOH₂²⁺** was calculated as the sum of the integrated charge under the Ru^{III}-OH/Ru^{II}-OH₂ and Ru^{III}-OOH/Ru^{II}-OOH waves. The latter is known as a surface-bound intermediate in the water oxidation cycle for the **RuPOH₂²⁺** catalyst.¹¹⁻¹⁴

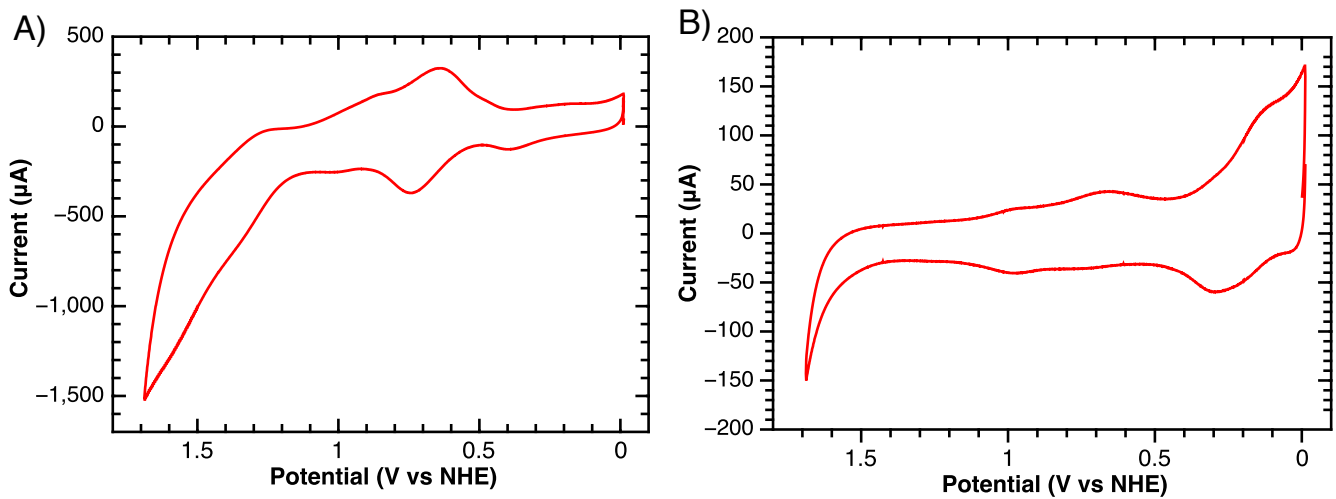


Figure S18. Cyclic voltammograms of **nITO-RuPdvb²⁺-polyRuOH₂²⁺** pre (A) and post 14 hr (B) electrolysis at 1.7 V (vs NHE) in pH 4.7 ((0.1 M HOAc/OAc, 0.5 M NaClO₄); Pt-mesh counter electrode and Ag/AgCl reference electrode. Surface coverages for both **RuPdvb²⁺** and **polyRuOH₂²⁺** were $\sim 1.1 \times 10^{-8}$ mol cm⁻² pre electrolysis. Following the 14 hr electrolysis, only $\sim 16\%$ of **polyRuOH₂²⁺** remained mainly as the peroxide intermediate.

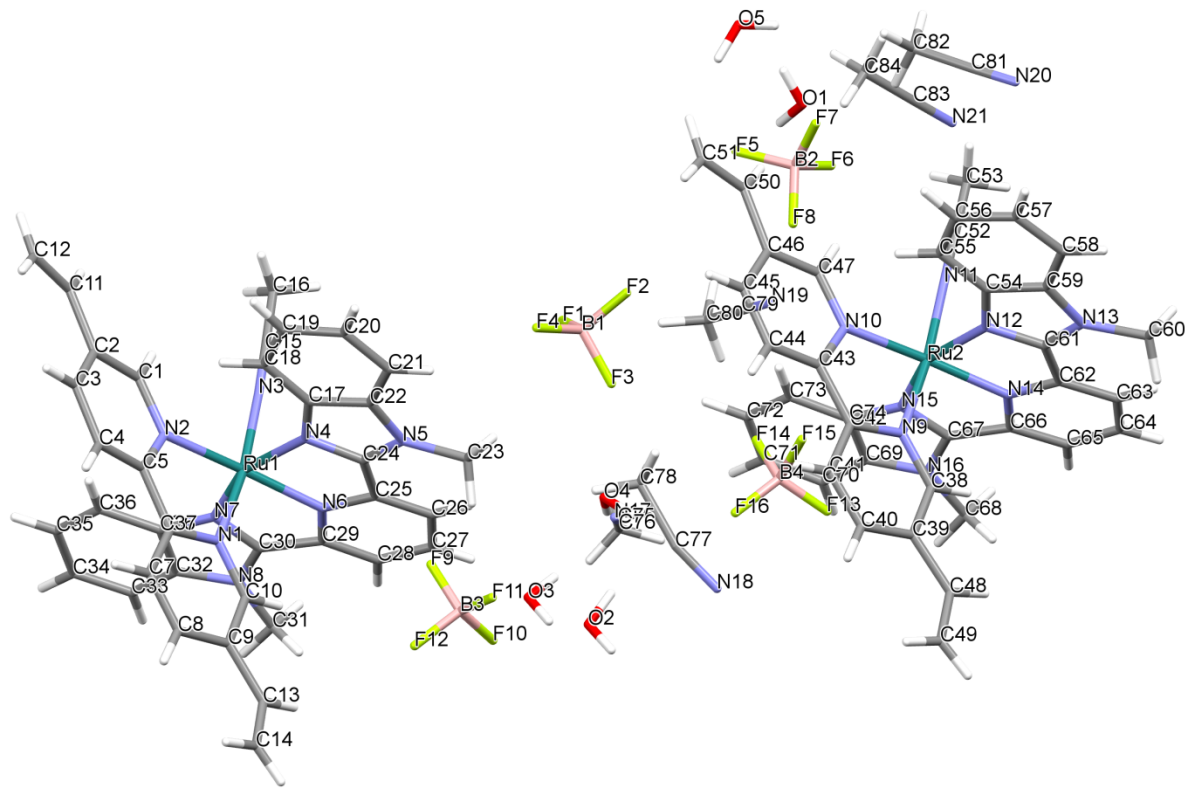


Table S1 Crystal data and structure refinement for DLA-3-216

Identification code	DLA-3-216
Empirical formula	C ₈₄ H ₈₉ B ₄ F ₁₆ N ₂₁ O ₅ Ru ₂
Formula weight	2022.14
Temperature/K	100.15
Crystal system	monoclinic
Space group	P2 ₁ /c
a/Å	19.0462(4)
b/Å	25.0845(6)
c/Å	19.0686(4)
α/°	90
β/°	92.458(2)
γ/°	90
Volume/Å ³	9101.9(3)
Z	4
ρ _{calc} mg/mm ³	1.476
m/mm ⁻¹	3.511
F(000)	4128.0
Crystal size/mm ³	0.461 × 0.13 × 0.042
2Θ range for data collection	4.644 to 140.488°
Index ranges	-19 ≤ h ≤ 23, -29 ≤ k ≤ 30, -20 ≤ l ≤ 22
Reflections collected	66621
Independent reflections	16885[R(int) = 0.0785]
Data/restraints/parameters	16885/18/1197
Goodness-of-fit on F ²	1.014

Final R indexes [I>=2σ (I)] $R_1 = 0.0687$, $wR_2 = 0.1660$
Final R indexes [all data] $R_1 = 0.1148$, $wR_2 = 0.1920$
Largest diff. peak/hole / e Å⁻³ 1.03/-0.69

Table S2 Fractional Atomic Coordinates ($\times 10^4$) and Equivalent Isotropic Displacement Parameters ($\text{\AA}^2 \times 10^3$) for DLA-3-216. U_{eq} is defined as 1/3 of the trace of the orthogonalised U_{IJ} tensor.

Atom	x	y	z	$U(\text{eq})$
Ru1	9389.8(2)	2275.1(2)	4468.3(2)	30.23(13)
N1	10388(3)	2239(2)	4892(2)	32.1(11)
N2	9470(3)	1473(2)	4712(3)	33.5(11)
N3	8384(3)	2203(2)	4075(3)	32.2(11)
N4	9013(3)	2529(2)	5417(2)	31.6(11)
N5	8751(3)	3226(2)	6092(3)	37.0(12)
N6	9367(2)	3065(2)	4330(3)	30.1(10)
N7	9746(2)	2350(2)	3460(2)	32.0(11)
N8	10076(3)	2896(2)	2611(3)	38.3(12)
C1	8969(3)	1091(3)	4602(3)	38.1(14)
C2	8997(4)	592(3)	4921(4)	40.9(15)
C3	9574(4)	484(3)	5369(3)	44.2(16)
C4	10102(4)	857(3)	5462(3)	40.8(15)
C5	10049(3)	1346(3)	5121(3)	35.3(13)
C6	10586(3)	1764(3)	5181(3)	35.2(13)
C7	11244(3)	1690(3)	5502(3)	40.7(15)
C8	11716(3)	2111(3)	5540(3)	42.5(16)
C9	11526(3)	2609(3)	5255(3)	37.4(14)
C10	10857(3)	2647(3)	4924(3)	35.7(13)
C11	8422(4)	208(3)	4766(4)	51.1(18)
C12	8327(4)	-245(3)	5092(5)	59(2)
C13	11981(3)	3081(3)	5292(4)	47.7(17)
C14	12581(4)	3118(4)	5636(5)	67(2)
C15	7823(3)	2139(3)	3876(3)	36.6(14)
C16	7105(3)	2054(3)	3609(4)	50.2(18)
C17	8783(3)	2334(3)	6047(3)	37.0(14)
C18	8673(3)	1812(3)	6275(3)	39.2(14)
C19	8396(4)	1745(3)	6927(3)	43.7(16)
C20	8253(4)	2189(3)	7357(3)	42.9(16)
C21	8356(3)	2706(3)	7147(3)	37.4(14)
C22	8618(3)	2772(3)	6481(3)	34.4(13)
C23	8692(4)	3773(3)	6353(4)	49.5(17)
C24	8975(3)	3065(3)	5460(3)	34.9(13)
C25	9117(3)	3383(3)	4835(3)	35.1(14)
C26	9008(4)	3919(3)	4727(4)	43.7(16)
C27	9160(4)	4136(3)	4072(4)	47.5(17)
C28	9430(4)	3811(3)	3567(4)	45.3(16)
C29	9535(3)	3275(3)	3704(3)	36.0(14)
C30	9796(3)	2855(3)	3242(3)	36.0(14)
C31	10282(4)	3383(3)	2246(4)	48.5(18)

C32	10210(3)	2389(3)	2386(3)	36.6(14)
C33	10482(4)	2193(3)	1769(4)	45.2(16)
C34	10546(4)	1660(3)	1704(4)	50.3(18)
C35	10329(4)	1297(3)	2239(4)	46.9(17)
C36	10059(3)	1482(3)	2851(3)	40.1(15)
C37	9999(3)	2037(3)	2913(3)	36.3(14)
Ru2	5109.5(2)	7343.9(2)	5400.8(2)	29.41(12)
N9	6128(3)	7325(2)	5793(2)	32.3(11)
N10	5228(3)	6536(2)	5600(3)	31.6(11)
N11	4094(3)	7282.4(19)	5029(2)	29.8(10)
N12	4743(3)	7567(2)	6363(3)	33.7(11)
N13	4433(3)	8232(2)	7066(3)	40.0(13)
N14	5056(3)	8136(2)	5291(3)	33.1(11)
N15	5447(3)	7450(2)	4391(3)	31.3(11)
N16	5775(3)	8011(2)	3557(3)	36.5(12)
C38	6565(3)	7737(3)	5840(3)	37.5(14)
C39	7247(3)	7701(3)	6125(3)	39.6(14)
C40	7474(4)	7212(3)	6373(4)	49.0(18)
C41	7037(4)	6779(3)	6323(4)	47.1(17)
C42	6350(3)	6838(3)	6019(3)	38.2(14)
C43	5855(3)	6396(3)	5942(3)	37.3(14)
C44	5957(4)	5885(3)	6180(4)	45.8(17)
C45	5452(4)	5504(3)	6073(4)	50.6(18)
C46	4829(4)	5634(3)	5702(4)	45.3(16)
C47	4748(3)	6155(3)	5477(3)	36.4(14)
C48	7679(3)	8190(3)	6167(4)	45.8(17)
C49	8321(4)	8232(4)	6439(5)	73(3)
C50	4246(4)	5254(3)	5559(4)	52.3(18)
C51	4212(5)	4774(3)	5819(5)	63(2)
C52	3525(3)	7246(3)	4840(3)	35.5(14)
C53	2804(3)	7206(3)	4576(4)	46.1(17)
C54	4509(3)	7344(3)	6974(3)	36.4(14)
C55	4420(3)	6816(3)	7172(3)	37.5(14)
C56	4141(4)	6723(3)	7825(4)	45.2(16)
C57	3966(3)	7146(3)	8270(3)	48.5(18)
C58	4047(3)	7671(3)	8077(4)	44.2(16)
C59	4320(3)	7762(3)	7421(3)	38.9(15)
C60	4317(4)	8771(3)	7346(4)	47.8(17)
C61	4673(3)	8096(3)	6430(3)	36.8(14)
C62	4806(3)	8434(3)	5821(4)	39.0(15)
C63	4678(4)	8974(3)	5720(4)	47.6(17)
C64	4805(4)	9204(3)	5080(4)	49.4(17)
C65	5081(4)	8902(3)	4549(4)	44.8(16)
C66	5215(3)	8365(3)	4674(3)	35.6(14)
C67	5481(3)	7958(3)	4198(3)	34.1(13)
C68	5949(4)	8519(3)	3204(4)	49.1(18)

C69	5884(3)	7505(3)	3312(3)	35.4(13)
C70	6159(3)	7321(3)	2689(3)	38.6(14)
C71	6187(3)	6779(3)	2600(3)	41.7(15)
C72	5962(3)	6421(3)	3118(3)	38.0(14)
C73	5711(3)	6606(3)	3741(3)	34.7(13)
C74	5680(3)	7152(2)	3836(3)	31.1(13)
F1	5366(5)	4858(3)	1401(4)	145(3)
F2	5060(4)	5121(4)	2481(4)	148(3)
F3	5983(6)	5364(4)	2068(5)	190(5)
F4	5832(7)	4528(4)	2325(5)	219(6)
B1	5556(6)	4944(4)	2061(6)	66(3)
F5	3297(4)	5388(2)	3471(4)	116(3)
F6	2949(3)	6231(2)	3350(3)	70.0(14)
F7	2873(3)	5803(3)	4389(3)	110(3)
F8	3931(3)	6014(3)	3992(3)	97(2)
B2	3260(5)	5862(4)	3816(6)	59(2)
F9	8750(8)	4519(4)	1913(5)	226(7)
F10	9202(4)	5303(2)	1749(3)	111(3)
F11	9056(5)	4987(2)	2827(3)	119(3)
F12	9764(5)	4617(5)	2170(7)	232(7)
B3	9166(6)	4875(4)	2159(5)	58(2)
F13	7913(4)	6646(2)	7888(3)	94(2)
F14	7400(3)	5890(2)	7503(3)	77.9(15)
F15	7496(3)	6080(3)	8664(3)	103(2)
F16	8454(3)	5862(2)	8149(3)	79.6(15)
B4	7837(6)	6131(5)	8005(6)	67(3)
O1	2055(4)	6007(3)	1981(3)	91(2)
O2	9418(8)	5558(8)	4784(8)	294(10)
O3	9770(4)	4787(3)	6002(5)	247(8)
O4	8870(4)	4778(3)	7896(5)	192(6)
O5	3548(4)	4102(3)	9153(5)	109(3)
N17	7953(10)	5525(5)	4077(8)	176(7)
C75	7819(8)	5663(5)	3483(10)	114(6)
C76	7677(7)	5804(6)	2763(9)	145(7)
N18	8802(5)	6266(4)	6208(5)	99(3)
C77	8551(7)	5790(6)	6190(7)	107(4)
C78	8032(12)	5308(8)	6086(12)	246(11)
N19	6443(6)	5234(4)	9575(6)	104(3)
C79	6518(6)	5107(4)	9003(8)	91(4)
C80	6576(7)	4968(5)	8239(7)	126(5)
N20	2979(5)	6447(4)	9831(5)	89(3)
C81	2948(5)	6103(4)	9472(5)	66(2)
C82	2888(6)	5636(4)	8989(6)	88(3)
N21	2687(4)	6640(3)	6156(4)	72(2)
C83	2703(4)	6221(4)	6364(5)	59(2)
C84	2718(6)	5683(4)	6633(8)	122(5)

Table S3 Anisotropic Displacement Parameters ($\text{\AA}^2 \times 10^3$) for DLA-3-216. The Anisotropic displacement factor exponent takes the form: $-2\pi^2[h^2a^{*2}\mathbf{U}_{11} + \dots + 2hkaxb\mathbf{U}_{12}]$

Atom	\mathbf{U}_{11}	\mathbf{U}_{22}	\mathbf{U}_{33}	\mathbf{U}_{23}	\mathbf{U}_{13}	\mathbf{U}_{12}
Ru1	26.2(2)	40.2(3)	24.1(2)	3.47(17)	-0.49(16)	-0.24(19)
N1	31(3)	43(3)	22(3)	0.0(19)	1.4(19)	3(2)
N2	34(3)	38(3)	29(3)	6(2)	6(2)	3(2)
N3	32(3)	37(3)	27(3)	2.8(19)	0(2)	4(2)
N4	32(3)	40(3)	23(3)	-2.4(19)	-2.7(19)	-1(2)
N5	35(3)	43(3)	33(3)	-1(2)	5(2)	2(2)
N6	21(2)	36(3)	32(3)	7(2)	-2.4(19)	-2(2)
N7	24(2)	51(3)	21(3)	1(2)	-0.6(18)	0(2)
N8	33(3)	51(3)	31(3)	7(2)	0(2)	-8(2)
C1	40(4)	44(4)	29(3)	2(2)	-5(3)	-3(3)
C2	48(4)	35(3)	41(4)	2(3)	7(3)	0(3)
C3	60(4)	41(4)	32(4)	4(3)	7(3)	7(3)
C4	43(4)	47(4)	33(4)	4(3)	3(3)	4(3)
C5	33(3)	46(4)	27(3)	1(2)	2(2)	7(3)
C6	33(3)	48(4)	25(3)	-2(2)	0(2)	4(3)
C7	40(4)	47(4)	35(4)	3(3)	3(3)	7(3)
C8	33(3)	65(5)	29(4)	2(3)	-8(3)	6(3)
C9	31(3)	59(4)	22(3)	1(3)	0(2)	-2(3)
C10	26(3)	50(4)	31(3)	1(3)	1(2)	-6(3)
C11	51(4)	48(4)	54(5)	0(3)	3(3)	-2(3)
C12	64(5)	45(4)	70(6)	-5(4)	11(4)	-9(4)
C13	33(3)	70(5)	40(4)	-3(3)	-2(3)	-3(3)
C14	48(5)	67(6)	83(7)	-8(4)	-22(4)	-4(4)
C15	31(3)	46(4)	33(3)	1(2)	3(3)	3(3)
C16	31(3)	70(5)	49(5)	0(3)	-3(3)	-2(3)
C17	28(3)	55(4)	28(3)	-2(3)	3(2)	-1(3)
C18	41(4)	46(4)	30(4)	4(3)	1(3)	-2(3)
C19	52(4)	52(4)	28(4)	0(3)	9(3)	-3(3)
C20	50(4)	51(4)	27(3)	2(3)	8(3)	6(3)
C21	38(3)	47(4)	27(3)	-3(3)	-1(2)	2(3)
C22	30(3)	45(4)	28(3)	1(2)	-2(2)	-2(3)
C23	63(5)	49(4)	37(4)	-4(3)	7(3)	2(4)
C24	28(3)	46(4)	31(3)	-1(2)	-1(2)	-2(3)
C25	30(3)	51(4)	24(3)	2(2)	0(2)	2(3)
C26	45(4)	41(4)	46(4)	4(3)	8(3)	-2(3)
C27	60(5)	40(4)	42(4)	9(3)	2(3)	-3(3)
C28	50(4)	47(4)	39(4)	11(3)	2(3)	-9(3)
C29	29(3)	50(4)	29(3)	5(3)	-5(2)	0(3)
C30	33(3)	46(4)	29(3)	9(2)	1(2)	-2(3)
C31	59(5)	49(4)	38(4)	5(3)	12(3)	-12(3)

C32	30(3)	50(4)	30(3)	1(3)	0(2)	-1(3)
C33	43(4)	61(5)	32(4)	5(3)	2(3)	-4(3)
C34	54(4)	66(5)	30(4)	-8(3)	4(3)	1(4)
C35	49(4)	48(4)	43(4)	-4(3)	0(3)	0(3)
C36	37(3)	50(4)	33(4)	3(3)	0(3)	-1(3)
C37	29(3)	49(4)	32(4)	3(3)	0(2)	3(3)
Ru2	29.1(2)	36.0(2)	23.0(2)	1.35(17)	-0.37(16)	-0.63(19)
N9	32(3)	39(3)	25(3)	1.2(19)	0.6(19)	2(2)
N10	34(3)	33(3)	27(3)	2.7(18)	3(2)	1(2)
N11	30(3)	32(3)	27(3)	1.1(18)	3.2(19)	0(2)
N12	29(3)	43(3)	28(3)	-3(2)	-5(2)	-4(2)
N13	40(3)	47(3)	33(3)	-11(2)	-3(2)	2(3)
N14	28(3)	41(3)	31(3)	-5(2)	-1(2)	-3(2)
N15	30(3)	38(3)	26(3)	3.8(19)	0.5(19)	-3(2)
N16	36(3)	41(3)	33(3)	6(2)	1(2)	-8(2)
C38	33(3)	49(4)	31(3)	-3(3)	1(2)	3(3)
C39	39(3)	54(4)	25(3)	-4(3)	1(2)	-1(3)
C40	34(4)	73(5)	40(4)	2(3)	-2(3)	3(3)
C41	44(4)	60(5)	37(4)	5(3)	0(3)	13(3)
C42	37(3)	51(4)	26(3)	4(2)	0(3)	2(3)
C43	41(4)	42(4)	29(3)	3(2)	5(3)	8(3)
C44	40(4)	55(4)	43(4)	13(3)	5(3)	9(3)
C45	57(5)	42(4)	54(5)	9(3)	9(4)	3(3)
C46	54(4)	42(4)	41(4)	4(3)	12(3)	0(3)
C47	40(3)	39(3)	31(3)	0(2)	9(3)	4(3)
C48	35(4)	67(5)	35(4)	-6(3)	-2(3)	-4(3)
C49	53(5)	82(7)	84(7)	-1(5)	-9(5)	-9(5)
C50	60(5)	45(4)	52(5)	-3(3)	8(4)	-3(4)
C51	78(6)	44(5)	66(6)	3(4)	-2(4)	-14(4)
C52	39(4)	44(4)	24(3)	2(2)	3(2)	4(3)
C53	28(3)	69(5)	41(4)	1(3)	-1(3)	-3(3)
C54	27(3)	57(4)	25(3)	-3(3)	-4(2)	4(3)
C55	34(3)	55(4)	24(3)	-5(2)	-3(2)	3(3)
C56	41(4)	61(5)	33(4)	0(3)	1(3)	-3(3)
C57	32(3)	90(6)	24(4)	-3(3)	4(3)	-4(3)
C58	29(3)	67(5)	36(4)	-9(3)	-5(3)	3(3)
C59	32(3)	52(4)	33(4)	-7(3)	-6(2)	-1(3)
C60	48(4)	47(4)	48(4)	-14(3)	-2(3)	3(3)
C61	31(3)	43(4)	36(4)	-5(3)	0(3)	-5(3)
C62	30(3)	43(4)	44(4)	-6(3)	2(3)	-5(3)
C63	48(4)	44(4)	51(5)	-4(3)	8(3)	-2(3)
C64	55(4)	37(4)	57(5)	1(3)	5(3)	-1(3)
C65	48(4)	40(4)	46(4)	1(3)	-5(3)	-8(3)
C66	33(3)	39(3)	35(4)	5(2)	0(3)	-7(3)
C67	27(3)	47(4)	28(3)	8(2)	-7(2)	-1(3)
C68	57(4)	47(4)	44(4)	16(3)	3(3)	-11(3)

C69	34(3)	44(4)	28(3)	5(2)	-1(2)	-2(3)
C70	33(3)	58(4)	25(3)	6(3)	4(2)	-2(3)
C71	40(4)	59(4)	27(3)	3(3)	4(3)	5(3)
C72	36(3)	46(4)	32(4)	-4(3)	1(3)	2(3)
C73	30(3)	47(4)	27(3)	5(2)	2(2)	4(3)
C74	27(3)	42(3)	24(3)	4(2)	-1(2)	0(2)
F1	234(10)	129(7)	68(5)	-27(4)	-28(5)	-55(6)
F2	131(7)	195(9)	122(7)	32(6)	55(5)	53(6)
F3	247(11)	203(10)	124(7)	-90(7)	61(7)	-134(9)
F4	365(16)	134(8)	156(9)	11(6)	1(9)	169(10)
B1	87(8)	52(6)	59(6)	-13(4)	-4(5)	23(5)
F5	121(5)	67(4)	157(7)	-26(4)	-42(5)	12(4)
F6	73(3)	69(3)	69(3)	16(2)	19(3)	7(3)
F7	93(4)	133(6)	106(5)	67(4)	52(4)	37(4)
F8	80(4)	165(6)	45(3)	20(3)	-12(3)	-58(4)
B2	55(5)	47(5)	75(7)	9(4)	21(5)	3(4)
F9	376(17)	190(10)	108(7)	20(6)	-34(9)	-186(11)
F10	248(8)	44(3)	41(3)	4(2)	4(4)	-19(4)
F11	242(9)	66(4)	51(4)	15(3)	35(4)	31(5)
F12	155(9)	297(14)	253(13)	153(11)	105(9)	130(9)
B3	73(7)	47(5)	56(6)	-10(4)	10(5)	6(5)
F13	155(6)	66(4)	59(4)	10(3)	-42(4)	-9(4)
F14	105(4)	74(4)	52(3)	-6(2)	-22(3)	-9(3)
F15	82(4)	155(7)	72(4)	-8(4)	-2(3)	-23(4)
F16	76(4)	77(4)	85(4)	10(3)	-13(3)	-1(3)
B4	53(5)	82(8)	66(7)	-17(5)	-7(5)	-4(5)
O1	120(6)	86(5)	67(5)	-4(4)	13(4)	24(4)
O2	188(14)	510(30)	186(16)	16(17)	6(12)	-103(16)
O3	265(16)	206(14)	262(17)	72(12)	-78(14)	-176(13)
O4	206(12)	88(7)	291(16)	-36(9)	120(11)	-12(8)
O5	62(4)	75(5)	189(9)	-7(5)	-12(5)	-6(4)
N17	300(20)	79(9)	157(14)	-7(8)	84(15)	4(11)
C75	127(11)	56(7)	166(16)	7(8)	73(12)	8(7)
C76	116(11)	134(14)	192(18)	58(12)	67(11)	56(10)
N18	96(6)	92(6)	106(6)	12(5)	-15(5)	9(5)
C77	113(6)	107(6)	102(6)	0(4)	7(4)	-14(4)
C78	249(14)	229(14)	262(14)	-10(9)	51(9)	-23(9)
N19	100(8)	102(8)	110(9)	22(6)	14(7)	31(6)
C79	69(7)	62(7)	144(12)	11(7)	33(8)	2(5)
C80	153(13)	81(9)	148(13)	-36(8)	57(10)	-40(9)
N20	99(7)	83(7)	84(7)	-16(5)	-12(5)	8(5)
C81	64(6)	67(6)	68(6)	1(4)	15(4)	8(5)
C82	119(9)	61(6)	88(8)	-7(5)	45(7)	-5(6)
N21	79(5)	76(6)	62(5)	0(4)	3(4)	7(4)
C83	56(5)	56(5)	67(6)	-2(4)	13(4)	-2(4)
C84	105(9)	57(7)	208(16)	37(8)	53(10)	21(6)

Table S4 Bond Lengths for DLA-3-216.

Atom	Atom	Length/Å	Atom	Atom	Length/Å
Ru1	N1	2.035(5)	N13	C59	1.382(9)
Ru1	N2	2.069(5)	N13	C60	1.472(8)
Ru1	N3	2.036(5)	N13	C61	1.358(8)
Ru1	N4	2.075(5)	N14	C62	1.358(8)
Ru1	N6	1.998(5)	N14	C66	1.356(8)
Ru1	N7	2.076(5)	N15	C67	1.329(8)
N1	C6	1.359(8)	N15	C74	1.383(7)
N1	C10	1.358(8)	N16	C67	1.374(8)
N2	C1	1.362(8)	N16	C68	1.486(8)
N2	C5	1.360(8)	N16	C69	1.371(8)
N3	C15	1.129(8)	C38	C39	1.389(9)
N4	C17	1.384(7)	C39	C40	1.379(10)
N4	C24	1.350(8)	C39	C48	1.475(10)
N5	C22	1.388(8)	C40	C41	1.369(10)
N5	C23	1.466(8)	C41	C42	1.415(9)
N5	C24	1.357(8)	C42	C43	1.459(9)
N6	C25	1.353(8)	C43	C44	1.371(9)
N6	C29	1.357(8)	C44	C45	1.366(10)
N7	C30	1.338(8)	C45	C46	1.394(10)
N7	C37	1.406(8)	C46	C47	1.382(9)
N8	C30	1.341(8)	C46	C50	1.480(10)
N8	C31	1.468(8)	C48	C49	1.312(10)
N8	C32	1.370(9)	C50	C51	1.305(10)
C1	C2	1.392(9)	C52	C53	1.446(9)
C2	C3	1.390(10)	C54	C55	1.389(9)
C2	C11	1.477(10)	C54	C59	1.407(9)
C3	C4	1.379(10)	C55	C56	1.394(9)
C4	C5	1.391(9)	C56	C57	1.409(10)
C5	C6	1.465(9)	C57	C58	1.378(10)
C6	C7	1.385(9)	C58	C59	1.394(9)
C7	C8	1.386(10)	C61	C62	1.468(9)
C8	C9	1.403(9)	C62	C63	1.390(9)
C9	C10	1.401(8)	C63	C64	1.380(10)
C9	C13	1.467(10)	C64	C65	1.387(10)
C11	C12	1.312(10)	C65	C66	1.390(9)
C13	C14	1.297(10)	C66	C67	1.469(9)
C15	C16	1.456(9)	C69	C70	1.397(8)
C17	C18	1.399(9)	C69	C74	1.402(8)
C17	C22	1.419(9)	C70	C71	1.371(9)
C18	C19	1.381(8)	C71	C72	1.414(9)
C19	C20	1.417(9)	C72	C73	1.381(8)

C20	C21	1.372(9)	C73	C74	1.384(9)
C21	C22	1.394(8)	F1	B1	1.312(12)
C24	C25	1.468(8)	F2	B1	1.339(12)
C25	C26	1.375(9)	F3	B1	1.331(14)
C26	C27	1.405(9)	F4	B1	1.263(12)
C27	C28	1.377(10)	F5	B2	1.362(11)
C28	C29	1.382(9)	F6	B2	1.398(11)
C29	C30	1.472(9)	F7	B2	1.352(10)
C32	C33	1.395(9)	F8	B2	1.362(11)
C32	C37	1.409(9)	F9	B3	1.270(13)
C33	C34	1.349(10)	F10	B3	1.331(11)
C34	C35	1.439(10)	F11	B3	1.330(11)
C35	C36	1.375(9)	F12	B3	1.310(12)
C36	C37	1.402(9)	F13	B4	1.319(13)
Ru2	N9	2.049(5)	F14	B4	1.381(11)
Ru2	N10	2.073(5)	F15	B4	1.446(12)
Ru2	N11	2.038(5)	F16	B4	1.372(12)
Ru2	N12	2.069(5)	N17	C75	1.20(2)
Ru2	N14	2.000(5)	C75	C76	1.43(2)
Ru2	N15	2.074(5)	N18	C77	1.287(15)
N9	C38	1.329(8)	C77	C78	1.57(2)
N9	C42	1.356(8)	N19	C79	1.150(16)
N10	C43	1.381(8)	C79	C80	1.507(17)
N10	C47	1.336(8)	N20	C81	1.100(12)
N11	C52	1.130(8)	C81	C82	1.491(12)
N12	C54	1.383(8)	N21	C83	1.125(11)
N12	C61	1.340(8)	C83	C84	1.443(12)

Table S5 Bond Angles for DLA-3-216.

Atom	Atom	Atom	Angle/[°]	Atom	Atom	Atom	Angle/[°]
N1	Ru1	N2	79.0 (2)	C38	N9	Ru2	126.0 (4)
N1	Ru1	N3	172.1 (2)	C38	N9	C42	119.5 (6)
N1	Ru1	N4	91.16 (19)	C42	N9	Ru2	114.5 (4)
N1	Ru1	N7	91.99 (18)	C43	N10	Ru2	114.8 (4)
N2	Ru1	N4	97.3 (2)	C47	N10	Ru2	126.7 (4)
N2	Ru1	N7	105.8 (2)	C47	N10	C43	118.3 (5)
N3	Ru1	N2	93.2 (2)	C52	N11	Ru2	178.2 (5)
N3	Ru1	N4	89.61 (19)	C54	N12	Ru2	140.4 (5)
N3	Ru1	N7	90.36 (19)	C61	N12	Ru2	113.0 (4)
N4	Ru1	N7	156.9 (2)	C61	N12	C54	106.5 (5)
N6	Ru1	N1	96.4 (2)	C59	N13	C60	125.2 (6)
N6	Ru1	N2	173.9 (2)	C61	N13	C59	106.8 (6)
N6	Ru1	N3	91.43 (19)	C61	N13	C60	128.0 (6)
N6	Ru1	N4	78.8 (2)	C62	N14	Ru2	119.1 (4)
N6	Ru1	N7	78.1 (2)	C66	N14	Ru2	119.9 (4)
C6	N1	Ru1	116.0 (4)	C66	N14	C62	120.8 (6)
C10	N1	Ru1	125.9 (4)	C67	N15	Ru2	113.6 (4)
C10	N1	C6	118.1 (5)	C67	N15	C74	106.6 (5)
C1	N2	Ru1	127.2 (4)	C74	N15	Ru2	139.7 (4)
C5	N2	Ru1	114.0 (4)	C67	N16	C68	126.4 (6)
C5	N2	C1	118.0 (5)	C69	N16	C67	106.7 (5)
C15	N3	Ru1	176.4 (5)	C69	N16	C68	126.9 (6)
C17	N4	Ru1	141.5 (4)	N9	C38	C39	123.3 (6)
C24	N4	Ru1	112.3 (4)	C38	C39	C48	118.5 (6)
C24	N4	C17	106.3 (5)	C40	C39	C38	117.7 (7)
C22	N5	C23	124.6 (6)	C40	C39	C48	123.7 (6)
C24	N5	C22	107.6 (5)	C41	C40	C39	120.0 (7)
C24	N5	C23	127.7 (6)	C40	C41	C42	119.7 (7)
C25	N6	Ru1	119.8 (4)	N9	C42	C41	119.6 (6)
C25	N6	C29	120.0 (6)	N9	C42	C43	117.4 (6)
C29	N6	Ru1	119.8 (4)	C41	C42	C43	123.0 (6)
C30	N7	Ru1	113.8 (4)	N10	C43	C42	113.4 (6)
C30	N7	C37	105.6 (5)	C44	C43	N10	120.1 (6)
C37	N7	Ru1	140.6 (5)	C44	C43	C42	126.5 (6)
C30	N8	C31	127.9 (6)	C45	C44	C43	121.0 (7)
C30	N8	C32	107.3 (5)	C44	C45	C46	119.4 (7)
C32	N8	C31	124.5 (6)	C45	C46	C50	123.9 (7)
N2	C1	C2	123.5 (6)	C47	C46	C45	117.4 (7)
C1	C2	C11	119.0 (7)	C47	C46	C50	118.7 (7)
C3	C2	C1	117.3 (6)	N10	C47	C46	123.7 (7)
C3	C2	C11	123.7 (6)	C49	C48	C39	126.6 (8)

C4	C3	C2	119.9(6)	C51	C50	C46	125.1(8)
C3	C4	C5	120.1(6)	N11	C52	C53	178.1(7)
N2	C5	C4	121.0(6)	N12	C54	C55	131.4(6)
N2	C5	C6	115.0(6)	N12	C54	C59	108.0(6)
C4	C5	C6	124.0(6)	C55	C54	C59	120.5(6)
N1	C6	C5	114.5(5)	C54	C55	C56	117.3(6)
N1	C6	C7	121.8(6)	C55	C56	C57	121.4(7)
C7	C6	C5	123.7(6)	C58	C57	C56	121.9(6)
C6	C7	C8	119.6(6)	C57	C58	C59	116.4(6)
C7	C8	C9	120.1(6)	N13	C59	C54	106.8(6)
C8	C9	C13	123.9(6)	N13	C59	C58	130.6(7)
C10	C9	C8	116.7(6)	C58	C59	C54	122.5(7)
C10	C9	C13	119.4(6)	N12	C61	N13	111.9(6)
N1	C10	C9	123.6(6)	N12	C61	C62	118.4(6)
C12	C11	C2	126.0(8)	N13	C61	C62	129.6(6)
C14	C13	C9	126.0(8)	N14	C62	C61	110.4(6)
N3	C15	C16	179.1(7)	N14	C62	C63	119.9(6)
N4	C17	C18	131.1(6)	C63	C62	C61	129.6(6)
N4	C17	C22	108.6(6)	C64	C63	C62	119.5(7)
C18	C17	C22	120.2(6)	C63	C64	C65	120.3(7)
C19	C18	C17	117.5(6)	C64	C65	C66	118.4(7)
C18	C19	C20	121.1(7)	N14	C66	C65	120.9(6)
C21	C20	C19	122.7(6)	N14	C66	C67	109.8(5)
C20	C21	C22	116.1(6)	C65	C66	C67	129.2(6)
N5	C22	C17	105.8(5)	N15	C67	N16	111.4(6)
N5	C22	C21	131.8(6)	N15	C67	C66	118.3(5)
C21	C22	C17	122.4(6)	N16	C67	C66	130.4(6)
N4	C24	N5	111.7(6)	N16	C69	C70	131.5(6)
N4	C24	C25	118.7(6)	N16	C69	C74	107.0(5)
N5	C24	C25	129.4(6)	C70	C69	C74	121.6(6)
N6	C25	C24	109.9(6)	C71	C70	C69	116.8(6)
N6	C25	C26	121.7(6)	C70	C71	C72	121.9(6)
C26	C25	C24	128.4(6)	C73	C72	C71	120.9(6)
C25	C26	C27	118.4(6)	C72	C73	C74	117.6(6)
C28	C27	C26	119.4(7)	N15	C74	C69	108.2(6)
C27	C28	C29	120.0(6)	N15	C74	C73	130.7(5)
N6	C29	C28	120.4(6)	C73	C74	C69	121.1(6)
N6	C29	C30	110.2(6)	F1	B1	F2	117.1(11)
C28	C29	C30	129.3(6)	F1	B1	F3	106.3(10)
N7	C30	N8	112.7(6)	F3	B1	F2	100.3(9)
N7	C30	C29	117.5(5)	F4	B1	F1	109.8(10)
N8	C30	C29	129.7(6)	F4	B1	F2	109.1(11)
N8	C32	C33	132.3(6)	F4	B1	F3	114.0(13)
N8	C32	C37	107.2(6)	F5	B2	F6	107.5(9)
C33	C32	C37	120.5(7)	F7	B2	F5	109.6(8)
C34	C33	C32	117.7(6)	F7	B2	F6	110.8(7)

C33	C34	C35	122.1(7)	F7	B2	F8	111.7(9)
C36	C35	C34	121.1(7)	F8	B2	F5	107.3(8)
C35	C36	C37	116.2(6)	F8	B2	F6	109.8(7)
N7	C37	C32	107.2(6)	F9	B3	F10	113.5(10)
C36	C37	N7	130.5(6)	F9	B3	F11	112.3(10)
C36	C37	C32	122.3(6)	F9	B3	F12	100.7(11)
N9	Ru2	N10	79.4(2)	F11	B3	F10	114.0(8)
N9	Ru2	N12	91.89(19)	F12	B3	F10	109.9(10)
N9	Ru2	N15	90.87(19)	F12	B3	F11	105.2(10)
N10	Ru2	N15	105.06(19)	F13	B4	F14	112.3(10)
N11	Ru2	N9	174.2(2)	F13	B4	F15	106.8(9)
N11	Ru2	N10	94.82(19)	F13	B4	F16	114.6(9)
N11	Ru2	N12	88.75(19)	F14	B4	F15	106.5(8)
N11	Ru2	N15	90.79(18)	F16	B4	F14	114.1(9)
N12	Ru2	N10	98.1(2)	F16	B4	F15	101.3(9)
N12	Ru2	N15	156.8(2)	N17	C75	C76	177.1(16)
N14	Ru2	N9	96.0(2)	N18	C77	C78	162.0(16)
N14	Ru2	N10	174.5(2)	N19	C79	C80	176.0(14)
N14	Ru2	N11	89.7(2)	N20	C81	C82	178.6(12)
N14	Ru2	N12	78.8(2)	N21	C83	C84	179.5(11)
N14	Ru2	N15	78.0(2)				

Table S6 Torsion Angles for DLA-3-216.

A	B	C	D	Angle/°	A	B	C	D	Angle/°
Ru1 N1 C6 C5	1.8(7)				Ru2 N9 C38 C39	178.6(4)			
Ru1 N1 C6 C7	-178.4(5)				Ru2 N9 C42 C41	-177.8(5)			
Ru1 N1 C10 C9	176.4(4)				Ru2 N9 C42 C43	1.5(7)			
Ru1 N2 C1 C2	-164.6(5)				Ru2 N10 C43 C42	-7.2(6)			
Ru1 N2 C5 C4	165.2(5)				Ru2 N10 C43 C44	171.8(5)			
Ru1 N2 C5 C6	-13.5(6)				Ru2 N10 C47 C46	-171.6(5)			
Ru1 N4 C17 C18	-5.1(12)				Ru2 N12 C54 C55	-1.1(11)			
Ru1 N4 C17 C22	178.1(5)				Ru2 N12 C54 C59	-178.4(5)			
Ru1 N4 C24 N5	-177.9(4)				Ru2 N12 C61 N13	-180.0(4)			
Ru1 N4 C24 C25	6.9(7)				Ru2 N12 C61 C62	4.5(7)			
Ru1 N6 C25 C24	6.7(7)				Ru2 N14 C62 C61	5.2(7)			
Ru1 N6 C25 C26	-171.6(5)				Ru2 N14 C62 C63	-171.5(5)			
Ru1 N6 C29 C28	171.1(5)				Ru2 N14 C66 C65	170.2(5)			
Ru1 N6 C29 C30	-6.8(7)				Ru2 N14 C66 C67	-5.9(7)			
Ru1 N7 C30 N8	175.3(4)				Ru2 N15 C67 N16	173.7(4)			
Ru1 N7 C30 C29	-5.6(7)				Ru2 N15 C67 C66	-6.1(7)			
Ru1 N7 C37 C32	-174.2(5)				Ru2 N15 C74 C69	-174.8(5)			
Ru1 N7 C37 C36	5.4(11)				Ru2 N15 C74 C73	7.3(11)			
N1 C6 C7 C8	0.8(10)				N9 C38 C39 C40	-0.4(9)			
N2 C1 C2 C3	-0.5(10)				N9 C38 C39 C48	-178.3(6)			
N2 C1 C2 C11	179.8(6)				N9 C42 C43 N10	3.8(8)			
N2 C5 C6 N1	7.9(8)				N9 C42 C43 C44	-175.1(6)			
N2 C5 C6 C7	-172.0(6)				N10 C43 C44 C45	1.3(10)			
N4 C17 C18 C19	-176.0(6)				N12 C54 C55 C56	-177.3(6)			
N4 C17 C22 N5	0.3(7)				N12 C54 C59 N13	1.0(7)			
N4 C17 C22 C21	178.5(5)				N12 C54 C59 C58	178.6(6)			
N4 C24 C25 N6	-8.9(8)				N12 C61 C62 N14	-6.3(8)			
N4 C24 C25 C26	169.3(6)				N12 C61 C62 C63	170.0(7)			
N5 C24 C25 N6	176.8(6)				N13 C61 C62 N14	179.1(6)			
N5 C24 C25 C26	-5.0(11)				N13 C61 C62 C63	-4.5(12)			
N6 C25 C26 C27	0.2(10)				N14 C62 C63 C64	0.1(11)			
N6 C29 C30 N7	8.0(8)				N14 C66 C67 N15	7.8(8)			
N6 C29 C30 N8	-173.2(6)				N14 C66 C67 N16	-172.0(6)			
N8 C32 C33 C34	-179.6(7)				N16 C69 C70 C71	-179.0(6)			
N8 C32 C37 N7	-0.8(7)				N16 C69 C74 N15	0.3(7)			
N8 C32 C37 C36	179.6(6)				N16 C69 C74 C73	178.5(5)			
C1 N2 C5 C4	-4.9(9)				C38 N9 C42 C41	2.0(9)			
C1 N2 C5 C6	176.4(5)				C38 N9 C42 C43	-178.7(5)			
C1 C2 C3 C4	-2.3(10)				C38 C39 C40 C41	1.2(10)			
C1 C2 C11 C12	-170.4(8)				C38 C39 C48 C49	177.7(8)			
C2 C3 C4 C5	1.5(10)				C39 C40 C41 C42	-0.4(10)			

C3 C2 C11 C12	9.8(12)	C40 C39 C48 C49	-0.1(12)
C3 C4 C5 N2	2.3(10)	C40 C41 C42 N9	-1.2(10)
C3 C4 C5 C6	-179.2(6)	C40 C41 C42 C43	179.5(6)
C4 C5 C6 N1	-170.7(6)	C41 C42 C43 N10	-176.9(6)
C4 C5 C6 C7	9.4(10)	C41 C42 C43 C44	4.2(10)
C5 N2 C1 C2	4.1(9)	C42 N9 C38 C39	-1.2(9)
C5 C6 C7 C8	-179.3(6)	C42 C43 C44 C45	-179.8(6)
C6 N1 C10 C9	-1.8(9)	C43 N10 C47 C46	3.2(9)
C6 C7 C8 C9	0.0(10)	C43 C44 C45 C46	1.5(11)
C7 C8 C9 C10	-1.6(9)	C44 C45 C46 C47	-1.9(10)
C7 C8 C9 C13	177.9(6)	C44 C45 C46 C50	-179.7(7)
C8 C9 C10 N1	2.6(9)	C45 C46 C47 N10	-0.5(10)
C8 C9 C13 C14	-6.4(12)	C45 C46 C50 C51	7.4(12)
C10 N1 C6 C5	-179.8(5)	C47 N10 C43 C42	177.4(5)
C10 N1 C6 C7	0.0(9)	C47 N10 C43 C44	-3.6(9)
C10 C9 C13 C14	173.1(8)	C47 C46 C50 C51	-170.4(8)
C11 C2 C3 C4	177.5(6)	C48 C39 C40 C41	179.0(6)
C13 C9 C10 N1	-177.0(5)	C50 C46 C47 N10	177.5(6)
C17 N4 C24 N5	1.6(7)	C54 N12 C61 N13	2.6(7)
C17 N4 C24 C25	-173.7(5)	C54 N12 C61 C62	-172.9(5)
C17 C18 C19 C20	-2.1(10)	C54 C55 C56 C57	-0.9(10)
C18 C17 C22 N5	-176.9(6)	C55 C54 C59 N13	-176.7(5)
C18 C17 C22 C21	1.2(9)	C55 C54 C59 C58	0.9(9)
C18 C19 C20 C21	2.2(11)	C55 C56 C57 C58	1.5(11)
C19 C20 C21 C22	-0.5(10)	C56 C57 C58 C59	-0.9(10)
C20 C21 C22 N5	176.4(7)	C57 C58 C59 N13	176.7(6)
C20 C21 C22 C17	-1.2(9)	C57 C58 C59 C54	-0.3(9)
C22 N5 C24 N4	-1.4(7)	C59 N13 C61 N12	-2.0(7)
C22 N5 C24 C25	173.2(6)	C59 N13 C61 C62	172.9(6)
C22 C17 C18 C19	0.5(9)	C59 C54 C55 C56	-0.2(9)
C23 N5 C22 C17	-176.2(6)	C60 N13 C59 C54	-178.7(6)
C23 N5 C22 C21	5.9(11)	C60 N13 C59 C58	4.0(11)
C23 N5 C24 N4	175.3(6)	C60 N13 C61 N12	177.2(6)
C23 N5 C24 C25	-10.1(11)	C60 N13 C61 C62	-7.9(11)
C24 N4 C17 C18	175.7(7)	C61 N12 C54 C55	175.3(6)
C24 N4 C17 C22	-1.1(7)	C61 N12 C54 C59	-2.1(7)
C24 N5 C22 C17	0.6(7)	C61 N13 C59 C54	0.5(7)
C24 N5 C22 C21	-177.3(6)	C61 N13 C59 C58	-176.8(6)
C24 C25 C26 C27	-177.7(6)	C61 C62 C63 C64	-175.9(7)
C25 N6 C29 C28	-2.2(9)	C62 N14 C66 C65	-4.5(9)
C25 N6 C29 C30	179.9(5)	C62 N14 C66 C67	179.4(5)
C25 C26 C27 C28	-1.7(11)	C62 C63 C64 C65	-2.1(11)
C26 C27 C28 C29	1.3(11)	C63 C64 C65 C66	0.8(11)
C27 C28 C29 N6	0.7(10)	C64 C65 C66 N14	2.5(10)
C27 C28 C29 C30	178.1(7)	C64 C65 C66 C67	177.7(6)
C28 C29 C30 N7	-169.7(6)	C65 C66 C67 N15	-167.9(6)

C28 C29 C30 N8	9.2(12)	C65 C66 C67 N16	12.4(11)
C29 N6	C25 C24 -179.9(5)	C66 N14 C62 C61	179.9(5)
C29 N6	C25 C26 1.8(9)	C66 N14 C62 C63	3.2(9)
C30 N7	C37 C32 1.4(7)	C67 N15 C74 C69	2.4(7)
C30 N7	C37 C36 -179.0(7)	C67 N15 C74 C73	-175.5(6)
C30 N8	C32 C33 178.3(7)	C67 N16 C69 C70	179.1(7)
C30 N8	C32 C37 -0.2(7)	C67 N16 C69 C74	-2.8(7)
C31 N8	C30 N7 -172.6(6)	C68 N16 C67 N15	-174.7(6)
C31 N8	C30 C29 8.5(11)	C68 N16 C67 C66	5.1(10)
C31 N8	C32 C33 -7.6(11)	C68 N16 C69 C70	-1.6(11)
C31 N8	C32 C37 173.9(6)	C68 N16 C69 C74	176.5(6)
C32 N8	C30 N7 1.2(7)	C69 N16 C67 N15	4.6(7)
C32 N8	C30 C29 -177.7(6)	C69 N16 C67 C66	-175.6(6)
C32 C33 C34 C35	1.5(11)	C69 C70 C71 C72	-1.3(10)
C33 C32 C37 N7	-179.5(6)	C70 C69 C74 N15	178.6(6)
C33 C32 C37 C36	0.8(10)	C70 C69 C74 C73	-3.2(9)
C33 C34 C35 C36	-1.5(12)	C70 C71 C72 C73	-0.7(10)
C34 C35 C36 C37	1.0(10)	C71 C72 C73 C74	0.7(9)
C35 C36 C37 N7	179.7(6)	C72 C73 C74 N15	178.9(6)
C35 C36 C37 C32	-0.7(10)	C72 C73 C74 C69	1.2(9)
C37 N7	C30 N8 -1.7(7)	C74 N15 C67 N16	-4.4(7)
C37 N7	C30 C29 177.4(5)	C74 N15 C67 C66	175.8(5)
C37 C32 C33 C34	-1.2(10)	C74 C69 C70 C71	3.2(9)

Table S7 Hydrogen Atom Coordinates ($\text{\AA} \times 10^4$) and Isotropic Displacement Parameters ($\text{\AA}^2 \times 10^3$) for DLA-3-216.

Atom	x	y	z	U(eq)
H1	8579	1170	4292	46
H3	9605	153	5610	53
H4	10501	780	5760	49
H7	11372	1353	5695	49
H8	12169	2062	5760	51
H10	10725	2976	4710	43
H11	8092	298	4398	61
H12A	8644	-352	5464	71
H12B	7940	-467	4955	71
H13	11822	3387	5040	57
H14A	12762	2821	5896	80
H14B	12840	3441	5629	80
H16A	7109	1918	3127	75
H16B	6847	2392	3613	75
H16C	6873	1794	3906	75
H18	8784	1514	5993	47
H19	8300	1396	7090	52
H20	8078	2127	7809	51
H21	8255	3001	7438	45
H23A	8285	3947	6119	74
H23B	9120	3971	6254	74
H23C	8631	3766	6861	74
H26	8833	4137	5087	52
H27	9078	4503	3978	57
H28	9544	3955	3126	54
H31A	10604	3291	1877	73
H31B	10517	3627	2581	73
H31C	9862	3556	2035	73
H33	10617	2426	1407	54
H34	10741	1519	1293	60
H35	10372	924	2168	56
H36	9921	1247	3210	48
H38	6403	8073	5670	45
H40	7935	7175	6580	59
H41	7193	6441	6492	57
H44	6387	5795	6423	55
H45	5524	5153	6249	61
H47	4327	6248	5220	44
H48	7470	8506	5979	55
H49A	8553	7928	6635	88

H49B	8553	8567	6441	88
H50	3868	5368	5254	63
H51A	4579	4645	6126	75
H51B	3819	4554	5701	75
H53A	2779	6979	4158	69
H53B	2626	7563	4454	69
H53C	2516	7051	4938	69
H55	4544	6531	6875	45
H56	4067	6366	7972	54
H57	3788	7068	8716	58
H58	3923	7956	8376	53
H60A	3871	8912	7149	72
H60B	4703	9005	7217	72
H60C	4300	8753	7858	72
H63	4503	9184	6089	57
H64	4704	9571	5004	59
H65	5176	9058	4109	54
H68A	5518	8681	3002	74
H68B	6273	8448	2829	74
H68C	6171	8764	3547	74
H70	6319	7560	2344	46
H71	6362	6640	2178	50
H72	5985	6048	3035	46
H73	5565	6367	4093	42
H1A	2243	5949	1581	136
H1B	1832	5723	2110	136
H2A	9648	5789	5046	441
H2B	8975	5643	4756	441
H3A	9391	4954	5854	371
H4A	9001	5017	8206	288
H4B	8883	4915	7477	288
H3B	10004	4987	6304	288
H5A	3999	4053	9143	164
H5B	3461	4352	9453	164
H76A	8084	5714	2489	218
H76B	7585	6187	2728	218
H76C	7265	5606	2580	218
H78A	7711	5377	5681	369
H78B	7762	5264	6508	369
H78C	8301	4982	6004	369
H80A	6105	4944	8014	189
H80B	6816	4625	8199	189
H80C	6845	5246	8008	189
H82A	3250	5660	8641	132
H82B	2422	5636	8750	132
H82C	2952	5307	9260	132

H84A	2572	5435	6257	183
H84B	2395	5654	7018	183
H84C	3196	5595	6806	183

Experimental

Single crystals of $C_{84}H_{89}B_4F_{16}N_{21}O_5Ru_2$ [DLA-3-216] were grown by solution diffusion of diethyl ether into a **RuOH₂** solution in CH₃CN resulting in CH₃CN coordination. A suitable crystal was selected and placed on a 'Bruker APEX-II CCD' diffractometer. The crystal was kept at 100.15 K during data collection. Using Olex2 [1], the structure was solved with the olex2.solve [2] structure solution program using Charge Flipping and refined with the ShelXL [3] refinement package using Least Squares minimisation.

O. V. Dolomanov, L. J. Bourhis, R. J. Gildea, J. A. K. Howard and H. Puschmann, OLEX2: a complete structure solution, refinement and analysis program. *J. Appl. Cryst.* (2009). 42, 339-341.

olex2.solve (L.J. Bourhis, O.V. Dolomanov, R.J. Gildea, J.A.K. Howard, H. Puschmann, in preparation, 2011)

SHELXL, G.M. Sheldrick, *Acta Cryst.* (2008). A64, 112-122

Crystal structure determination of [DLA-3-216]

Crystal Data for $C_{84}H_{89}B_4F_{16}N_{21}O_5Ru_2$ ($M=2022.14$): monoclinic, space group P2₁/c (no. 14), $a = 19.0462(4)$ Å, $b = 25.0845(6)$ Å, $c = 19.0686(4)$ Å, $\beta = 92.458(2)^\circ$, $V = 9101.9(3)$ Å³, $Z = 4$, $T = 100.15$ K, $\mu(\text{CuK}\alpha) = 3.511$ mm⁻¹, $D_{\text{calc}} = 1.476$ g/mm³, 66621 reflections measured ($4.644 \leq 2\Theta \leq 140.488$), 16885 unique ($R_{\text{int}} = 0.0785$) which were used in all calculations. The final R_1 was 0.0687 ($I > 2\sigma(I)$) and wR_2 was 0.1920 (all data).

This report has been created with Olex2, compiled on Apr 9 2013 14:10:59. Please let us know if there are any errors or if you would like to have additional features.

- (1) Bennett, M. A.; Smith, A. K. *J. Chem. Soc., Dalton Trans.* **1974**, 233.
- (2) Concepcion, J. J.; Jurss, J. W.; Norris, M. R.; Chen, Z. F.; Templeton, J. L.; Meyer, T. J. *Inorg. Chem.* **2010**, 49, 1277.
- (3) Liu, Y.; Zhang, S.; Miao, Q.; Zheng, L.; Zong, L.; Cheng, Y. *Macromolecules (Washington, DC, United States)* **2007**, 40, 4839.
- (4) Lee, S.-H. A.; Abrams, N. M.; Hoertz, P. G.; Barber, G. D.; Halaoui, L. I.; Mallouk, T. E. *J. Phys. Chem. B* **2008**, 112, 14415.
- (5) Gallagher, L. A.; Serron, S. A.; Wen, X.; Hornstein, B. J.; Dattelbaum, D. M.; Schoonover, J. R.; Meyer, T. J. *Inorg. Chem.* **2005**, 44, 2089.
- (6) Connelly, N. G.; Geiger, W. E. *Chem. Rev.* **1996**, 96, 877.
- (7) Vannucci, A. K.; Hull, J. F.; Chen, Z.; Binstead, R. A.; Concepcion, J. J.; Meyer, T. J. *J. Am. Chem. Soc.* **2012**, 134, 3972.
- (8) Hanson, K.; Brennaman, M. K.; Luo, H.; Glasson, C. R. K.; Concepcion, J. J.; Song, W.; Meyer, T. J. *ACS Appl. Mater. Interfaces* **2012**, 4, 1462.
- (9) Norris, M. R.; Concepcion, J. J.; Glasson, C. R. K.; Fang, Z.; Lapides, A. M.; Ashford, D. L.; Templeton, J. L.; Meyer, T. J. *Inorg. Chem.* **2013**, 52, 12492.
- (10) Ashford, D. L.; Song, W. J.; Concepcion, J. J.; Glasson, C. R. K.; Brennaman, M. K.; Norris, M. R.; Fang, Z.; Templeton, J. L.; Meyer, T. J. *J. Am. Chem. Soc.* **2012**, 134, 19189.
- (11) Vannucci, A. K.; Alibabaei, L.; Losego, M. D.; Concepcion, J. J.; Kalanyan, B.; Parsons, G. N.; Meyer, T. J. *Proc. Nat. Acad. Sci.* **2013**, 110, 20918.
- (12) Concepcion, J. J.; Tsai, M. K.; Muckerman, J. T.; Meyer, T. J. *J. Am. Chem. Soc.* **2010**, 132, 1545.
- (13) Chen, Z. F.; Concepcion, J. J.; Hull, J. F.; Hoertz, P. G.; Meyer, T. J. *Dalton Trans.* **2010**, 39, 6950.
- (14) Chen, Z. F.; Vannucci, A. K.; Concepcion, J. J.; Jurss, J. W.; Meyer, T. J. *Proc. Nat. Acad. Sci. U.S.A* **2011**, 108, E1461.